# Chiral Symmetry Breaking via Computer Simulation

[FOMMS 2015 keynote address, July 12, 2015, Mt. Hood, Oregon:
45 min. formal presentation + 15 min. discussion]

Molecular chirality ("handedness") has fundamental relevance to pre-biotic terrestrial geochemistry. It is a feature of basic organic chemistry and of specific commercial interests that arise in the pharmaceutical industry. Furthermore it constitutes an important subject in chemical physics and condensed matter physics. These obvious features have been the source of many experimental and theoretical research investigations. However this fascinating area is still far from a fully understood subject. Consequently my Princeton collaborators and I have developed a strong interest in the phenomenon of spontaneous chiral symmetry breaking at the molecular level. This has led us to develop a three-dimensional continuum model that has demonstrated a capacity to exhibit this phenomenon. We have begun to examine that model in depth both analytically and with molecular dynamics computer simulation. This lecture will present descriptive details of that model, and will provide some of the numerical results which have emerged thus far from our efforts that are still in an early stage and very much underway.

==========

View 1. Title, coauthors, affiliations, financial support.

==========

Perhaps the best-known examples of broken chiral symmetry in our environment are exhibited by biopolymers, including the polynucleotides (DNA, RNA), polysaccharides (*e.g.*, cellulose), and polypeptides (proteins). Focusing for the moment on the last of these, there are twenty basic amino acids that serve as monomeric building blocks for protein linear polymerization via peptide linkages. Nineteen of the twenty primary amino acids have energy-equivalent distinct left and right hand mirror-image isomers. That basic handedness (chirality) stems from the nonplanar arrangement of four covalent chemical bonds emanating from the amino acids' $\alpha$-carbon stereocenter (C*), which is retained upon protein formation. But with overwhelming dominance only one of the two chiralities (enantiomers) for each of those nineteen appear in terrestrial living organisms. This is illustrated in the next View 2 for the simple amino acid

==========

View 2. Alanine enantiomers, with biological preference indicated.

==========

alanine. The minimum energy barrier to inversion of the alanine molecule in isolation, from one enantiomer to its mirror image, has been estimated to be approximately 130 kcal/mol [Lee, Shin, and Ka, J. Molec. Structure (Theochem), **679**, 59-63 (2004)]. The other amino acids are distinguished from alanine by replacement of the methyl group with different chemical groups chemically bonded to the C*.

How this chiral bias arose billions of years ago on our planet, and whether it was a necessary condition for the emergence and evolution of terrestrial life, have long been sources of speculation and argument. It has been tempting for astrophysicists to speculate that anything resembling life as we define it, occurring elsewhere in the universe, would be based on carbon chemistry, and would need chiral symmetry breaking to avoid being bogged down by useless and/or harmful molecular "trash". It seems to be generally accepted that if all biomolecules were simultaneously replaced by their mirror images the result would be a viable life form, leading some to speculate that such a scenario might exist somewhere else in the Universe. Examples of past proposals as to how our own broken chiral symmetry may have been produced are indicated in View 3. We may never know with

==========

View 3. Historically prominent proposals for terrestrial chiral symmetry breaking. [For the third case, a general hypothesis proposed by F.C. Frank (1953) became demonstrated as a chemical reaction in the laboratory by K. Soai, *et al.* (1995).]

==========

absolute certainty the historical truth about what actually happened on our planet, predating or during first appearance of life as we know it. However, rigorous scientific study of alternative hypothetical scenarios may ultimately allow assignment of relative probabilities to each of those and any other possible scenarios. What will be described in this lecture is just a modest single contribution to illustrate one aspect of chiral symmetry breaking that might have been involved in our planet's evolution, if only indirectly.

As illustrated in the earlier View 2, chiral distinctions for amino acids (and many other organic molecules) basically involve the relative spatial arrangement of five chemical units. These are a carbon stereocenter (C*) and four distinguishable units (ligands) stably arranged around that carbon in a non-planar pattern of tetrahedrally directed chemical bonds. In order for such a carbon stereocenter and its chemically bonded surroundings to undergo continuous conversion to its mirror image the structure must be forced to pass through a transition state that lies between distinguishable D and L configurations. Such a transition state by definition must be

indistinguishable from its mirror image. If this conversion were somehow to occur for an amino acid essentially in isolation, there are at least three geometrically distinct transition state patterns. Those three differ according to the sequential order around the C* into which the four surrounding ligands have been distorted from a tetrahedral to a planar arrangement.

But it's important to realize that in the broader chemical-physics context, molecular chiral distinctions can also arise in a simpler geometric scenario, an alternative that is exploited in the model to be described. This scenario is possible with just four centers (instead of five) which do not include a C* stereocenter, and which do not need to be fully distinguishable chemically. A familiar substance which illustrates this simpler molecular situation is hydrogen peroxide, $H_2O_2$ . Its stable left- and right-handed isolated-molecule geometries are illustrated in the next View 4. The *trans* energy

==========

View 4. Stable mirror-image structures for an isolated $H_2O_2$ molecule. The magnitude of the dihedral angle is $111.5^o$ for both structures.

==========

barrier to inversion between these mirror image configurations is thought to be approximately 1.1*kcal/mol*, while the *cis* barrier is somewhat larger at approximately 7*kcal/mol* [Hunt, *et al.*, J. Chem. Phys. **42,** 1931-1946 (1965)]. The chemically related substance hydrogen disulfide $H_2S_2$ has a similar pair of mechanically stable chiral geometries for its isolated molecules. The *cis* and *trans* rotation barriers for $H_2S_2$ are estimated to be somewhat larger than those for $H_2O_2$ .

The following View 5 shows that the hydrogen peroxide molecules

==========

View 5. Hydrogen peroxide tetragonal single crystal structure [Abraham, Collin, and Lipscomb, Acta Cryst. **4**, 15-20 (1951)]. Only the oxygen atoms are explicitly shown, but a hydrogen bond helix is indicated by dashed lines between oxygen atoms.

==========

crystallize in a periodic tetragonal pattern (m.p. $-0.41^\circ C$) as determined by single-crystal X-ray and neutron diffraction experiments. The unit cell in this structure contains four $H_2O_2$ molecules. The crystal appears to be stabilized primarily by hydrogen bonds and to be enantiopure. In other words, all of the molecules contained in a single crystal apparently share the same mirror image structure. This conclusion stems from the crystallographic observation that the tetragonal structure in a single crystal is penetrated by hydrogen bond helices all of the same handedness. One of

these helices (right-handed) is located spatially in View 5 by dashed lines. Of course energetically equivalent enantiopure crystals can form individually from molecules of the opposite chirality, and would display hydrogen bond helices of the opposite left-handedness. It should be noted that neutron diffraction measurements indicate that intermolecular interactions present in the crystal reduce the intramolecular dihedral angle from $111.5^o$ to $90.2^o$ [Busing and Levy, J. Chem. Phys. **42**, 3054-3059 (1965)].

With these observations as a background, an elementary tetramer model inspired very roughly by the hydrogen peroxide case can now be defined for the study of chirality phenomena, and some of its basic many-particle properties will be described. This is a three-dimensional continuum ("off-lattice") model. View 6 displays the mirror image pair of tetramers at their

==========

View 6. Mirror image pair of three-bond tetramers at their mechanically stable shapes in isolation.

==========

equivalent mechanically stable shapes (potential energy minima) when in isolation. These have a common bond length *b* for the three backbone bonds, two $90^\circ$ bond angles ($\theta_2$ and $\theta_3$) along that backbone, and a $\pm 90^\circ$ dihedral angle ($\varphi$). For the purpose of molecular dynamics simulation to be described the model assumes that each of the four monomers contained in a tetramer have a common mass *m*. It should be emphasized at the outset that this model is definitely not intended to be a computational replica of the hydrogen peroxide system, but rather it is intended to provide insight into certain aspects of the general chiral symmetry breaking subject.

The following View 7 indicates the algebraic format chosen to represent

==========

View 7. Intramolecular deformation potential energy $\Phi^{(1)}$ form, including definition of dihedral angle $\cos\varphi$.

==========

how the intramolecular potential energy $\Phi^{(1)}$ of a tetramer increases as that tetramer undergoes a deformation away from one of its two energetically equivalent mechanically stable ($\Phi^{(1)} = 0$) configurations. Notice that no explicit interactions between any of the three non-bonded pairs of centers (monomer units along the backbone) are included; the other interactions make that unnecessary. Notice also that chemical dissociation of the tetramers is not permitted in this format. Because the dihedral angle $\varphi$ only

appears in $\Phi^{(1)}$ as the even function $\cos^2\varphi$, mirror image symmetry is preserved and the stable structures are those shown in the preceding View 6.

An isolated tetramer possesses two planar transition states that exist between the configuration sets corresponding to the distinguishable enantiomers. This compares to at least three transition states expected for a carbon stereocenter as mentioned earlier. These two tetramer transition states are illustrated in View 8; they correspond to dihedral angles $\varphi = 0^\circ$,

==========

View 8. Planar transition states containing undeformed bond lengths and bond angles; their common activation energy is $K_{dih}$ relative to the minima.

==========

and to $\varphi = \pm 180^\circ$. Their respective shapes would conventionally be labeled "*cis*" and "*trans*" by chemists, but might informally be called an "incomplete square" and a "crank handle" by others. The bond lengths $r_{12}, r_{23}, r_{34}$ and bond bending angles $\theta_2, \theta_3$ remain unchanged from their values at the mechanically stable potential energy minima. These transition states are simple saddle points in the six-dimensional space of tetramer relative configurations, with only one negative curvature direction (the reaction path), while other intramolecular displacement directions in that tetramer configuration space have positive curvatures. The energy of activation for an isolated tetramer is just the parameter $K_{dih}$; it is the same for both transition states because only $\cos^2\varphi$ is involved. If one were motivated to remove this transition-state energy degeneracy, it would suffice to augment the $\cos^2\varphi$ term in the dihedral angle portion of the intramolecular potential energy with a $\cos\varphi$ contribution (which is still an even function of $\varphi$, preserving degeneracy of mirror-image configurations). Presuming that this additional contribution has suitably limited magnitude, the transition states with different heights would still occur at $\varphi = 0^\circ$ and at $\varphi = \pm 180^\circ$. However this would also cause the stable tetramer structures (the $\Phi^{(1)}$ minima) to have their dihedral angles shifted away from $\varphi = \pm 90^\circ$.

A rather simple mathematical way exists to distinguish the two tetramer enantiomers, even when they sustain substantial intramolecular deformations. This is accomplished by means of a scalar chirality measure $\zeta$ applicable to any single tetramer, regardless of its configuration. This quantity is defined in the following View 9. Its numerical values are confined to the interval

==========

View 9. Tetramer chirality measure $\zeta$.

==========

$-1 \le \zeta \le +1$, and are continuous functions of the tetramer's intramolecular deformations. It vanishes when the tetramer to which it is applied deforms to any planar configuration, including both of the pure transition states. Any pair of mirror-image enantiomers, regardless of their corresponding states of intramolecular deformation, possess the same magnitude of $\zeta$, but differ by algebraic sign. The fact that $\zeta$ can distinguish mirror image configurations stems from the fact that the numerator in its definition contains a product consisting of an odd number (3) of vectors (as opposed to their absolute values appearing in the denominator, which thus remains unchanged under mirror-imaging).

At this point it should be mentioned that a correspondingly simple basic chirality measure apparently does not exist for a carbon stereocenter C* and the four distinguishable ligands covalently attached to it. This is due to the more complicated enantiomer classification formalism that is required for five centers as opposed to just four in the tetramer model being presented here.

The next issue to consider is how the model postulates an intermolecular interaction $\Phi^{(2)}$ between a pair of distinct tetramers $\alpha$ and $\gamma$. As the following View 10 indicates this involves assigning Lennard-Jones 12,6 pair

==========

View 10. Pairwise additive intermolecular tetramer interactions $\Phi^{(2)}$; dependence of Lennard-Jones interaction strengths $\varepsilon_{tt}$ on the tetramer $\zeta^{(\alpha)}, \zeta^{(\gamma)}$ values involved.

==========

interactions between all 16 possible pairs of force centers (monomer vertices), with one on each of the two tetramers $\alpha$ and $\gamma$. A key feature of our model is that the Lennard-Jones energy parameter $\varepsilon_{tt}$ is postulated to depend on the two tetramers' chirality measures $\zeta^{(\alpha)}$ and $\zeta^{(\gamma)}$. This renormalization attribute permits control over whether the model energetically favors tetramer pairs of the same chirality or of the opposite chirality when they are nearby and interact, determined by the sign of the dimensionless coupling strength parameter $\lambda$. Specifically, for isolated tetramer pairs, $\lambda > 0$ biases $\Phi^{(2)}$ in favor of like enantiomers, $\lambda < 0$ biases in favor of opposite enantiomers. The Lennard-Jones length parameter $\sigma_{tt}$

however remains invariant to the $\zeta$'s. Note also that the form of the contribution of any monomer unit pair to $\Phi^{(2)}$ does not distinguish chain end monomers from chain interior monomers. In all of the results to be shown here, the dimensionless parameter $\lambda$ has been restricted to the values 0.5 and $-0.5$.

No higher-order molecular interactions (3-molecule, 4-molecule,....) are included in the model. Consequently the total potential energy $\Phi$ for any collection of tetramers simply consists of a sum of all $\Phi^{(1)}$ and $\Phi^{(2)}$ contributions present in the system. This implies for thermal equilibrium states that the system's energy and virial pressure can formally be expressed in terms of integrals involving 1-molecule and 2-molecule equilibrium distribution functions. Those expressions contain important intramolecular and intermolecular contributions from the spatial distributions of the tetramer bonds.

The next View 11 presents an illustrative specific choice of tetramer

==========

View 11. Parameter choice, physical units.

==========

interaction parameters that were selected informally while initiating our modeling study. As shown, these are expressed in real units, and were assigned in part to be rough order-of-magnitude values for the $H_2O_2$ molecule to assist physical insight. However it must be stressed that subsequently our simulations have been performed as conventionally the case in terms of dimensionless parameters, and indeed the specific physical-unit choices shown in View 11 can be trivially rescaled into dimensionless form. For this purpose the quantities $m, \varepsilon_0, \sigma_{tt}$ were selected as the elementary scaling set of parameters. The following View 12 indicates how

==========

View 12. Parameter choice, reduced units, scaling set $m, \varepsilon_0, \sigma_{tt}$.

==========

these three immediately define units of time, number density, temperature, and pressure. It also presents the corresponding dimensionless values of the parameters assigned to the intramolecular interaction potential $\Phi^{(1)}$. Results to be presented for our model will now be expressed in these reduced units, and will refer only to the reduced $\Phi^{(1)}$ interaction set shown in View 12. Longer-term investigation would naturally involve examining how independent variations in the four dimensionless $\Phi^{(1)}$ interactions would modify the model's properties.

It should be mentioned that in the numerical calculations to be reported which involve properties of condensed matter many-particle systems, the Lennard-Jones pair interactions have been subjected to a conventionally invoked radial cutoff simplification. This cutoff is imposed at $r = 2.5\sigma_{tt}$, with a linear function of $r$ added inside the cutoff to assure continuity of the resulting modified potential and its first *r* derivative at the cutoff. Applying this simplification speeds the molecular dynamics computations. However its effect is quantitatively relatively small, and should not qualitatively influence any of the conclusions to be presented. Longer term, it may be desirable to restore the full Lennard-Jones interaction form for some selected calculations.

An elementary illustration of the tetramer pair interaction effect appears in the following View 13. This shows the absolute energy minimum

==========

View 13. Tetramer pair absolute energy minimum structure for $\lambda = 0.5$, $\Phi = -13.18$. The tetramers are the same enantiomer. No substantial tetramer deformation is present. The tetramers occupy equivalent positions in this complex. [L-J cutoff at $2.5\sigma_{tt}$ in effect.]

==========

configuration for a pair of tetramers in isolation under the influence of a like-enantiomer bias $\lambda = 0.5$ in $\Phi^{(2)}$. As expected this absolute minimum is indeed attained with both tetramers the same enantiomer. The configuration shown of course has a mirror image twin comprising the opposite pair of identical enantiomers. The rather compact spatial arrangement of the eight monomer nodes can be viewed as a somewhat distorted version of the eight vertices of a simple cube, where the distortion involved is primarily a modest relative twist applied to the tetramers. The binding energy $-13.18$ for the twisted pair shown would be only $-10.14$ if the eight monomers were precisely confined to the vertices of an edge-*b* cube. These observations will be recalled later.

View 14 provides the corresponding absolute energy minimum

==========

View 14. Tetramer pair absolute energy minimum structure for $\lambda = -0.5$, $\Phi = -12.86$. The tetramers are opposite enantiomers. No substantial tetramer deformation is present. The tetramers occupy inequivalent positions in this complex. [L-J cutoff at $2.5\sigma_{tt}$ in effect.]

==========

configuration for $\lambda = -0.5$ in which the two tetramers are opposite enantiomers, *i.e.*, a "racemic" pair. Notice that this is a less compact

geometry, and exhibits somewhat less binding strength compared to the preceding $\lambda = 0.5$ case. This distinction could be interpreted as indicating that the model implicitly incorporates a bias toward enantiopurity. Both the like-enantiomer and the opposite-enantiomer arrangements just shown in Views 13 and 14 were inferred from many $\Phi$ minimizations for each $\lambda$ choice that were started with a large set of randomly generated initial configurations.

The one remaining set of interactions to be specified concerns how a nonchiral solvent might reasonably be included in the model. We have taken the most elementary position by assuming that solvent particles are structureless, and that Lennard-Jones 12,6 pair interactions act between solvent particle pairs, as well as between solvent particles and the monomer vertices in the tetramers. Details are presented in View 15. In the interest

==========

View 15. Tetramer-solvent and solvent-solvent pair interactions, including values selected for $\varepsilon_{ts}, \varepsilon_{ss}, \sigma_{ts}, \sigma_{ss}$ .

==========

of maximum simplicity for the computations that have been carried out thus far, we have assumed that the solvent-monomer interactions do not distinguish tetramer end monomers from tetramer internal monomers. Furthermore these interactions are assumed to be independent of the intramolecular deformations of the tetramers (*i.e.*, independent of bond lengths, bond and dihedral angles, and thus of the $\zeta$'s). Finally we have set $\varepsilon_{ts} = \varepsilon_{ss} = \varepsilon_0$ (= 0.15535 kcal/mol in physical units) and $\sigma_{ts} = \sigma_{ss} = \sigma_{tt}$ (= 1.115Å in physical units). Note also that each solvent particle is given the same mass *m* that has been assigned to monomers in the tetramers.

Once this solvation possibility has been defined, very basic initial molecular dynamics simulations are in order. Specifically this includes observing the rates of chiral interconversion as temperature varies for a single tetramer suspended in liquid solvent at thermal equilibrium. View 16

==========

View 16. $\varphi(t)$ for a single tetramer in solvent, two reduced temperatures $T = 4.0$ and 2.0 [L-J temperature unit = $\varepsilon_0 / k_B$ = 78.151K, time unit = $(m/\varepsilon_0)^{1/2}\sigma_{tt}$ = 0.4033ps]. $N_s = 4092$ solvent particles present at reduced number density $N_s \sigma_{tt}{}^3 / V = 0.6617$ . [Total L-J center density 0.6624]

==========

presents typical dihedral angle $\varphi(t)$ results for two runs at a fixed system volume but different temperatures. The patterns displayed indicate short-

term configurational persistence of one of the enantiomers, then sudden transition to the other enantiomer as a result of the stochastic collisional influence of the surrounding solvent. A strong temperature dependence of the interconversion rate is obvious, roughly 100 times faster for $T = 4.0$ compared to $T = 2.0$.

An alternative way of accessing the transition kinetics for a single dissolved tetramer is presented in View 17. This involves the time

==========

View 17. $\langle \zeta(t_0 + t)\zeta(t_0) \rangle / \langle \zeta^2(t_0) \rangle$ for the two different temperature runs in View 16. Rebound effect at $T = 4.0$, persistence at $T = 2.0$. The $T = 4.0$ case involved 35 runs, the $T = 2.0$ case involved 39 runs.

==========

dependence of the autocorrelation function for the enantiomer identifier $\zeta$, showing in a different way the persistence time of this chirality measure at the same two temperatures and system volume. The plots do not exhibit smooth decay, but instead appear to show the contribution of a transition "rebound" effect. In other words the many-body dynamics of transition state surface crossing occasionally has the tetramer almost immediately reversing direction and recrossing that surface in the opposite direction, most likely resulting from collision with one or more solvent particles. In addition, the lower temperature case indicates the presence of a few cases with long-term persistence of chirality.

As mentioned above, the results presented in these last two Views 16 and 17 indicate that raising the temperature isochorically from $T = 2$ to $T = 4$ causes the net transition rate to increase by approximately a factor of 100. This is consistent with rough classical transition state rate estimates at those two temperatures for the case of energy barriers equal to 17.86 in reduced units.

Although by construction the intramolecular potential energy barriers have the same height for the two distinguishable transition states possessed by a single tetramer, their respective solvation characteristics will tend to differ. This arises from the distinct tetramer shapes shown earlier for the *cis* and *trans* planar transition states which would tend to give rise to differing local solvent particle arrangements. That can influence the relative rates of passing through the two transition geometries. The detailed time dependences of $\varphi(t)$ and $\zeta(t)$ for a solvated tetramer allow the separate rates for these two transition state kinetic alternatives to be disentangled. Specifically this involves identifying the times at which $\zeta(t)$ passes through

zero, and determining whether $\varphi(t)$ at that instant is closer to $0^\circ$ or to $\pm 180^\circ$. View 18 shows numerical results for the resolved relative

==========

View 18. Resolved relative racemization rates through the two transition states for single dissolved tetramer. In this plot the two bar heights at each temperature sum to 1.0 .

==========

racemization rates exhibited by a single dissolved tetramer during two molecular dynamics runs at the same pair of reduced temperatures $T = 4.0$ and $T = 2.0$, and the same solvent density. Notice that the transition rate is substantially higher for the *cis* (incomplete square) transition state versus the *trans* (crankshaft) transition state at both temperatures, and that lowering the temperature enhances this difference.

Characterizing the statistical behavior of many simultaneously interacting tetramers, whether with or without solvent present, is a challenging but intriguing task. A recently reported experimental result adds a novel impetus to pursuing many-tetramer behavior in this model. View 19

==========

View 19. C. Dressel, *et al.*, *Nature Chemistry* **6**, 971-977 (2014), "Chiral self-sorting and amplification in isotropic liquids of achiral molecules". Includes an image of the 138-atom organic substance forming the coexisting immiscible chiral liquids.

==========

identifies the publication reference involved. It reveals the existence of an immiscible pair of chiral liquid phases that are formed from a nominally achiral organic substance comprised of flexible molecules without added solvent. These immiscible liquids rotate polarized light in opposite directions, and they coexist below a consolute temperature ($205^\circ$C), above which (presumably) a single racemic (achiral) isotropic liquid exists. View 20 presents photographs under polarized light showing that coexistence in a

==========

View 20. Fig. 2 photo(s) from the C. Dressel, *et al.* reference. The relative amount of light transmitted by the two phases as shown can be changed by adjusting the angle between the polarizer (P) and the analyzer (A) as indicated at the lower left of each photo. Sample thickness is approximately $15 \mu$m .

==========

thin film for several distinguishable macroscopic regions between which there are intervening sharp interfaces. Evidently these rather complicated

flexible molecules find it advantageous locally to pack together in one or a reversed mirror image mode that displays locally a consistent chiral deformation. However it needs to be emphasized that the two resulting liquids individually are isotropic: The molecular orientations across each homogeneous and isotropic macroscopic phase do not coherently define an orientational order parameter. This is confirmed by the fact that rotating the samples (at fixed polarizer and analyzer relative orientations) does not change the observed relative brightness of the two phases. For this reason the result needs to be distinguished from what are traditionally called "chiral liquid crystals."

The earlier View 19 illustrated the 138-atom molecule in an extended version that would be consistent with achirality. However the mechanically stable (potential energy minimum) structures for one of these isolated molecules have not been determined. It seems reasonable to suppose that they may include somewhat folded conformations that are chiral, and thus paired with mirror images. In this respect this substance may be roughly analogous to $H_2O_2$ and to our model tetramer.

Our tetramers do not possess either the extended cylindrical shape or the thin discotic shape that appear frequently to underlie liquid crystal formation. However their intrinsic chirality-producing flexibility strongly suggests that with appropriate interaction parameter choice (specifically $\lambda > 0$) our model could also exhibit immiscible chiral liquid phases, and that those phases would be isotropic, and respectively would consist primarily of opposite enantiomers. This would be closely similar to the situation reported in the View 19 reference. It should be mentioned in passing that the liquid phase separation described in that reference is roughly analogous to the phase transition exhibited by an Ising model as it is cooled below its critical temperature. Whether side-by-side coexistence of immiscible liquids would be observed in simulations for our model or whether only a single chiral liquid phase would be present at thermal equilibrium would depend (among other attributes) on the applicable rate of racemization.

To help determine if our model can in principle produce analogous immiscible liquid results, several solvent-free molecular dynamics runs for dense tetramer systems were performed. For these runs the intermolecular interaction bias parameter was again set at $\lambda = 0.50$. This was deliberately chosen so that the ratio of inter-tetramer Lennard-Jones coupling strengths $\varepsilon_{tt}$ for like versus unlike enantiomers could attain the extreme value 3, thus very strongly favoring contacts between like enantiomers. Of course if $T$

were sufficiently high this bias wouldn't matter, and the thermodynamic state would remain uniformly racemic. View 21 presents the time

==========

View 21. $N_{tetr}^{-1} \sum_{i=1}^{N_{tetr}} \zeta_i(t)$ plotted against *t*, for a high $T = 4.0$, $N_{tetr} = 1024$, tetramer density = 0.17 (more precisely 0.6624/4 = 0.1656). The initial state ($t = 0$) had all $\zeta_i(0) \cong 1$, *i.e.*, essentially undeformed tetramers of identical chirality.

==========

dependence of the chirality measures $\zeta_i(t)$ for one such high temperature state, averaged over the $N_{tetr} = 1024$ tetramers present. In spite of imposing an enantiopure initial liquid configuration, the result at long time clearly exhibits an approach to, and a fluctuation about, zero without any perceptible subsequent long-term drift. In other words at this temperature and density the system statistically prefers to be in a racemic state. This long-time behavior is demonstrably independent of any accidental or intentional enantiomeric excess present in the initial condition with which the molecular dynamics run began, as just illustrated.

Lowering the temperature a moderate amount for such runs naturally causes the average chirality measure (essentially an enantiomorphic excess measure) versus time to approach, and to fluctuate more slowly about, zero. At some stage of further cooling the fluctuation is observed to drift consistently away from zero, indicating essentially permanent system-wide dominance by one of the enantiomers over the other. That is, at this lowered temperature, free energy is minimized by displacing the enantiomeric excess one way or the other away from zero (the racemic state).

To display clearly the statistical driving force to break chiral symmetry at lower *T*, View 22 shows the time dependences of $N_{tetr}^{-1} \sum_{i=1}^{N_{tetr}} \zeta_i(t)$ for a

==========

View 22. $N_{tetr}^{-1} \sum_{i=1}^{N_{tetr}} \zeta_i(t)$ for a set of 20 molecular dynamics runs at lower temperature $T$=1.4 , all with an identical racemic initial configuration but with variable initial velocities from a Maxwell-Boltzmann distribution. Reduced tetramer density = 0.17 . Two of the runs are highlighted in red for clarity and to emphasize the symmetry breaking phenomenon. $N_{tetr} = 1024$ .

==========

collection of 20 independent molecular dynamics runs. These all started at identically the same system racemic (ee=0) configuration (a pair of enantiopure liquids separated by a planar interface) but with different initial monomer velocities chosen from a Maxwell-Boltzmann distribution corresponding to the lowered reduced temperature $T = 1.4$. Notice that the drift away from the initial racemic state appears to go randomly in either direction of chiral symmetry breaking, but once started it tends to continue in the same direction. Notice that a small minority of the cases have yet to exhibit a tendency to drift toward positive or negative final ee values. These exceptions may be due to persistence of approximately equal-sized opposite-chirality clusters, with net ee cancelation over the time interval examined, without yet showing development of final dominance of one chirality over the other. The other runs suggest that the final average chirality (ee) for this temperature and density should be approximately $\pm 0.6$.

View 23 presents the same type of ee decline from an enantiopure initial

==========

View 23. $N_{tetr}^{-1} \sum_{i=1}^{N_{tetr}} \zeta_i(t)$ plotted against *t*, for a lower *T* = 1.4, but same $N_{tetr} = 1024$ and density (0.17) as in View 21. The initial condition was also enantiopure as in View 21.

==========

state as in the earlier View 21, but for the substantially lower temperature $T = 1.4$ that applied in the immediately preceding View 22. This illustrates the dramatic decrease in rate of approach from initial enantiopurity to a "final" ee state. In the earlier View 21 the ee decay was substantially complete at $t = 200$, but here the final fluctuating condition is not yet obvious at $t = 20{,}000$. Aside from the selection of sign of the preferred chirality by choice of initial condition, the expected eventual statistical state is what chiral symmetry breaking in the preceding View 22 revealed, and indeed the plot shown has just attained the value +0.6 at its endpoint. The evident persistence of chiral bias at $T = 1.4$ places this temperature substantially below the liquid-liquid phase separation critical temperature (upper consolute temperature) for the imposed density 0.17.

The final result of cooling toward absolute zero temperature, assuming thermal equilibrium is maintained, would be freezing. In order to move toward a comprehensive understanding of our model for chiral symmetry breaking it is necessary eventually to determine the $T = 0$ stable crystal structures as a function of number density, and their corresponding melting

point temperatures. As a modest first step toward this goal we have started by considering a "prototype crystal" for enantiopure tetramers (with $\lambda = 0.5$) as illustrated in the following View 24. This involves filling all of the sites

==========

View 24. Enantiopure tetramers ($\lambda = 0.5$) whose monomers occupy the lattice sites of a simple cubic lattice. The tetramer number density in reduced units is $(\sigma_{tt}/b)^3/4 = 0.2109$, and the potential energy is $\Phi/N_{tetr} = -20.6595$. Only a single row of occupied cubes is shown for simplicity, but the potential energy per tetramer is for the entire simple cubic lattice, amounting to lateral replication of the row shown, to fill the entire available space.

==========

of a simple cubic lattice with single monomers, taking advantage of the $90^o$ angles of undeformed tetramers. The nearest-neighbor spacing in that simple cubic lattice is just the equilibrium bond length *b* of the tetramers. Notice that pairs of these tetramers occupy the vertices of a single basic cube in the lattice. It is worth recalling that the lowest energy structure for two like-enantiomers at $\lambda = 0.5$ shown earlier in View 13 amounts to a relatively modest distortion of that eight-vertex cube occupancy configuration.

However subsequent computation showed (not surprisingly) that this "prototype crystal" serving as an initial configuration was not mechanically stable and thus was not a proper $T = 0$ crystal structure for the model with the assigned interaction parameters. Beginning with a low temperature and low pressure ($T = 0.01$, $p = 0.01$) molecular dynamics run with 128 tetramers initially in the "prototype crystal" arrangement, followed by energy minimization, an alternative crystal structure finally appeared. It is illustrated by three orthogonal projections in Views 25, 26, and 27. Not

==========

View 25. Tentatively stable crystal inherent structure for $\lambda = 0.5$, $\rho_{tetr} = 0.24$, $p = 0.01$, $\Phi/N_{tetr} = -29.1$, projected along the x axis.

==========

==========

View 26. Tentatively stable crystal structure, projected along the y axis.

==========

==========

View 27. Tentatively stable crystal structure, projected along the z axis.

==========

only has the number density increased, but the neighboring paired tetramers have undergone small rotational changes similar to what was observed

earlier for the isolated enantiopure tetramer pair, View 13. These rotated tetramer pairs comprise the unit cell content of the final periodic structure. It should also be mentioned that this process has transformed the initial cubic configuration into a tetragonal structure with the x coordinate direction shrinking by about 1% compared to the other two perpendicular directions. This can be traced back to the corresponding structural asymmetry in the initial prototype configuration as can be verified by examining the schematic in View 24.

It should be noted in passing that other initial configurations were also considered in searching for the low-pressure stable crystal. One case was a body-centered cubic version of the simple cubic prototype, consisting of an interpenetrating pair of tetramer-occupied simple cubic sublattices. The corresponding results from molecular dynamics relaxation at low temperature and pressure, followed by potential energy minimization, invariably created configurations higher in potential energy than the structure illustrated in Views 25, 26, and 27.

Along with the series of liquid phase runs, this qualitatively completes initial probing of the portion of the phase diagram concerning the spontaneous chiral symmetry breaking phenomenon with pure tetramers at $\lambda = 0.5$. A correspondingly qualitative diagram in the enantiomeric excess, temperature plane, for low to modest pressure, is presented in View 28. It is

==========

View 28. Qualitative diagram in the enantiomeric excess, temperature plane for symmetry breaking when $\lambda > 0$, under isobaric conditions and with equilibrated racemization kinetics. The pressure is moderate but high enough to avoid vaporization over the temperature range included.

==========

presumed here that the pressure is nevertheless high enough for the temperature range plotted that vaporization has been avoided. Note the presence of an upper consolute point (critical point) as the system is cooled isobarically. It is reasonable to expect that this singularity has critical exponents similar, if not identical, to those describing conventional liquid-vapor critical points as well as the three-dimensional Ising model's critical point. In particular there may be a heat capacity divergence as the consolute point is approached either from above or below in temperature. These questions justify carrying out a sequence of fixed density and/or fixed pressure molecular dynamics runs with systematic small temperature steps to determine singular behavior of the various intensive properties as the consolute point is passed.

Note that the $\lambda < 0$ version of View 28 is trivial. There is no consolute

point at which the vertical racemic locus at high temperature splits into left and right hand chiral loci. Instead there would just be the single vertical locus at vanishing enantiomeric excess, even as a freezing transition to a racemic crystal may occur that would require relabeling of that vertical racemic locus: $l_0 \rightarrow c_0$ . It should also be acknowledged that at lower tetramer number density and over some temperature range the racemic liquid (like the enantiopure liquid) may also exhibit its own distinct "conventional" liquid-vapor critical point with a racemic vapor.

Although the choice $\lambda > 0$ favors enantiopurity under modest pressures, it is important to realize that a basic reversal to favoring racemic mixtures will occur with the same $\lambda$ choice under extreme pressure. This stems from the fact that the $\varepsilon_{tt}$ attractive well enhancement produced by $\lambda > 0$ for like enantiomers also enhances the strength of the repulsive core of the L-J monomer-monomer pair interactions. This is illustrated qualitatively in View 29. Consequently it becomes unfavorable to have tetramers with the

==========

View 29. Chirality-renormalized pair potential.

==========

same chirality very close together with $\lambda > 0$. In the very high pressure (very high density) limit, the stable $T = 0$ crystal would be expected to have a close-packed structure of repulsive cores, perhaps in an approximate FCC or HCP arrangement. The potential energy of such a many-tetramer configuration would be minimized by having as many monomers from opposite chirality tetramers as possible in close proximity, *i.e.*, maximizing opposite-enantiomer nearest-neighbor intermolecular monomer pairs on some appropriate kind of close-packed structure. That is, increasing pressure when $\lambda > 0$ should eventually cause a spontaneous transition to a racemic crystal state. This phenomenon would be reversed for $\lambda < 0$: The racemic $T = 0$ crystal structure expected at low pressure would be forced by elevated pressure to undergo spontaneous symmetry breaking toward one or the other enantiopure compositions!

By increasing $K_{dih}$ substantially it is possible at a fixed temperature effectively to eliminate racemization. Under this circumstance it is feasible to maintain essentially at thermal equilibrium an overall "racemic" state at low temperature even when $\lambda > 0$, but with spatial separation of two equal-sized immiscible phases in contact at an intervening interface. This situation would be analogous to the photograph shown earlier in View 20 for immiscible organic liquid films. View 30 shows an instantaneous view of a

==========

View 30. Side-by-side phase coexistence, immiscible chiral liquids, $T = 1.4$, $\rho_{tetr} = 0.17$, vanishing racemization rate due to increasing $K_{dih}$ by a factor 10 to 178.6, visible planar interface pair due to periodic boundary conditions, zero enantiomeric excess. [$N_+ = N_- = 512$]

==========

system in such a condition at $T = 1.4$, kinetically stabilized by increasing $K_{dih}$ by a factor of 10. On account of the length scale involved, individual tetramers are represented simply by small oriented squares, respectively red or blue depending on chirality. A detailed examination of the pair of parallel interfaces shows a small tendency for enantiomer penetration across the interface toward the phase of opposite chirality. It also shows a tetramer (*i.e.*, monomer) depletion in the interface due to reduced L-J attractions between the opposite enantiomers there. It should additionally find that the tetramer intramolecular bonds in the interface zone do not have isotropic direction distributions. This planar interface possesses a positive surface tension, that is, a positive free energy above what would be present for a single phase with the given bulk enantiomeric excess and number density. Although it has not yet been pursued, it would certainly be worthwhile to determine the temperature and pressure dependences of this planar interface surface tension.

If suddenly the enhanced $K_{dih}$ were then reduced by the same factor 10 to its previous value to re-establish racemization kinetics, the two contacting phases would begin to compete against each other for overall dominance. The thermodynamic driving force is the positive interface free energy. However this is a stochastic process that at low to moderate temperature could take a very long time for completion, at which just one of the chiral liquids finally fills the entire available volume. The problem is that any net interconversion will primarily occur at the interface, a small fraction of a large system. Furthermore a planar interface doesn't have a geometrically natural direction to move kinetically in favoring one phase over the other.

Nevertheless, in principle there is apparently a way to accelerate this liquid phase chiral dominance (beyond further numerical adjustment of $K_{dih}$). It amounts to establishing a parallel for our liquid phases to the "Ostwald ripening" phenomenon for crystals of variable sizes, a well-established behavior which is outlined in the following View 31. The

==========

View 31. Ostwald ripening phenomenon for crystals; Gibbs-Thompson effect; application to liquid droplets.

==========

underlying Gibbs-Thompson effect applies both to the analogous cases of small liquid droplets suspended in a surrounding macroscopically immiscible liquid medium, as well as to collections of small crystals in a fluid medium. These scenarios both involve radius-dependent increases in chemical potentials, thus destabilizing small crystals or droplets in favor of larger versions. This occurs spontaneously without interference from outside the system, but usually proceeds quite slowly, especially as the crystals or droplets increase in size toward the macroscopic limit. [Historical note: Wilhelm Ostwald was awarded the 1909 Nobel Prize in Chemistry (unshared) for his contributions to catalysis, chemical equilibria, and reaction rates.]

By implementing some kind of vigorous stirring in our model system that has been cooled so as to produce two coexisting immiscible liquids, the total interface area would increase dramatically while becoming nonplanar and disconnected. This would cause a substantial increase in the overall chiral inversion rate. Such irreversible treatment of the system will amount to a liquid-phase analog of "Viedma ripening", a well-established experimental technique for accelerating and completing deracemization of a crystal slurry composed of equal portions of left and right handed enantiopure crystals by vigorous stirring with glass beads. The following View 32 provides literature references for this phenomenon. For the present

==========

View 32. Viedma ripening references.

==========

model's immiscible liquids this should speed up the trend toward a single chiral phase with its characteristic enantiomorphic excess. How best to implement such a stirring process, and how long and vigorously it should be applied in a simulation remain open problems for future investigation.

With respect to other future investigations involving this model, the straightforward extensions that examine the effects of varying the input (reduced) interaction parameters $K_{str}, K_{bnd}, K_{dih}, b, \lambda$ have already been mentioned. Perhaps more interesting cases might include examination of the self diffusion constant $D$ and shear viscosity $\eta$ of both the racemic and symmetry-broken states, and to see to what extent the Stokes-Einstein relation is satisfied. As already mentioned the liquid-liquid surface tension needs to be determined as the upper consolute point for chiral symmetry breaking is approached from below in temperature. Another basic challenge would be to calculate the polarized light rotation produced by the chiral-symmetry-broken liquids, after assigning anisotropic polarizability to the

tetramers' covalent bonds. These research opportunities just identified for the model are listed in View 33.

==========

View 33. Tetramer Model: Future Applications

==========

Beyond these focused directions for future work on our specific tetramer model as presented, there is a broader context to which it might contribute involving a range of nagging questions about our prebiotic terrestrial biochemistry, alluded to briefly in the opening remarks. Listing a few of the corresponding wider research opportunities in the last View 34 is an appropriate way formally to end this presentation.

==========

View 34. Future research opportunities.

==========

[Name of generic program used for molecular dynamics and for potential energy minimizations: LAMMPS]

# Chiral Symmetry Breaking via Computer Simulation

Folarin B. Latinwo and Pablo G. Debenedetti,

Department of Chemical and Biological Engineering,
Princeton University;

and

Frank H. Stillinger,

Department of Chemistry, Princeton University

Financial support:
National Science Foundation Grant No. CHE-1213343

View 2

BACK

# AMINO ACID EXAMPLE: ALANINE

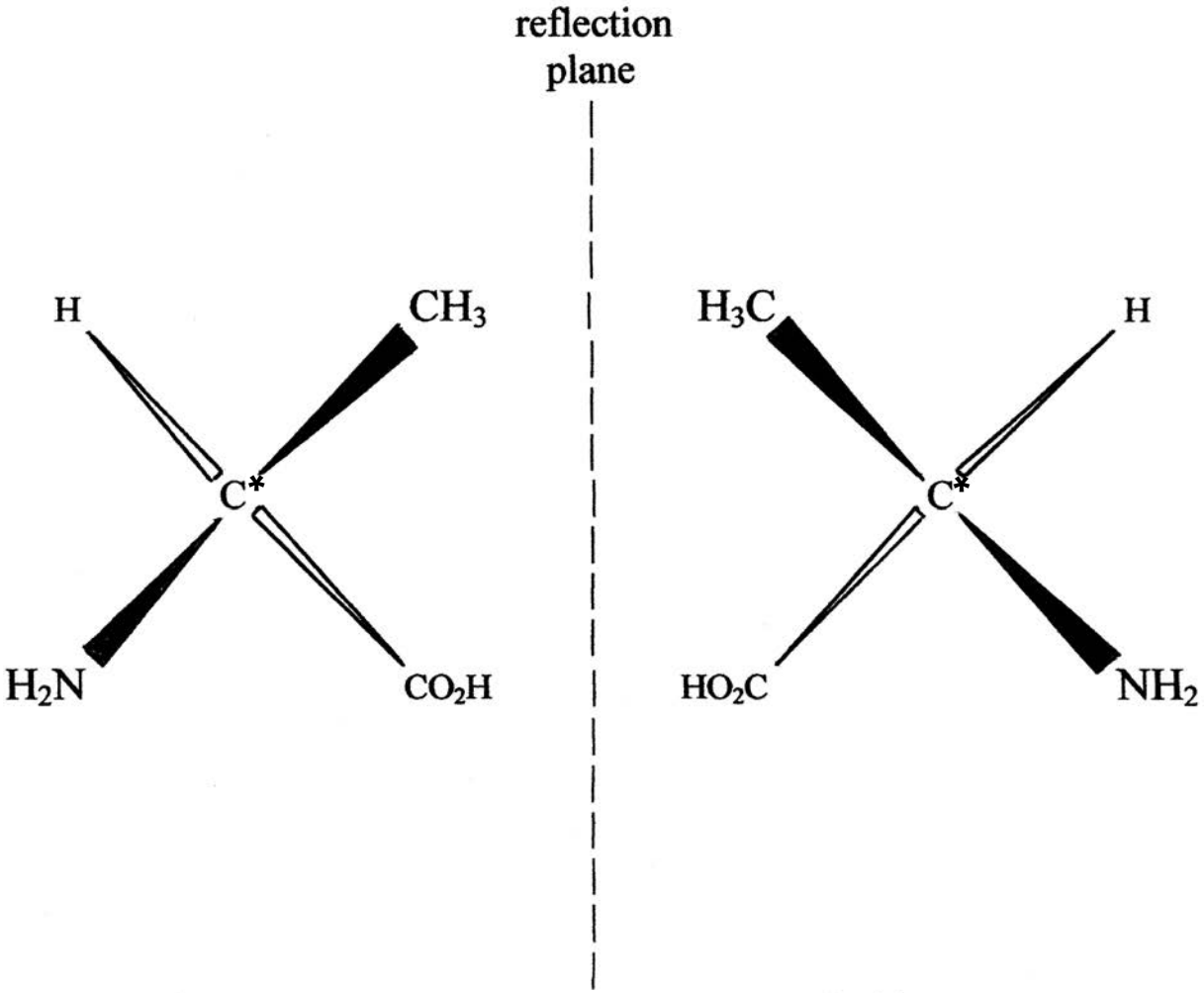


"L" isomer

**biologically favored**

"D" isomer

## Proposed Mechanisms for Chiral Symmetry Breaking

(1) Parity-violating weak interactions

(2) Chemical reactants illuminated with circularly polarized light

(3) Liquid-phase chemical kinetics with autocatalysis and heteroinhibition

(4) D,L phase diagram characterisitics: Amplification of enantiomorphic excess resulting from off-symmetry eutectic pairs

(5) Mechanically disturbed crystallization (stirring) with slow liquid-phase D,L interconversion, and "Ostwald ripening"

# Hydrogen Peroxide Stable Structures

View 4

BACK

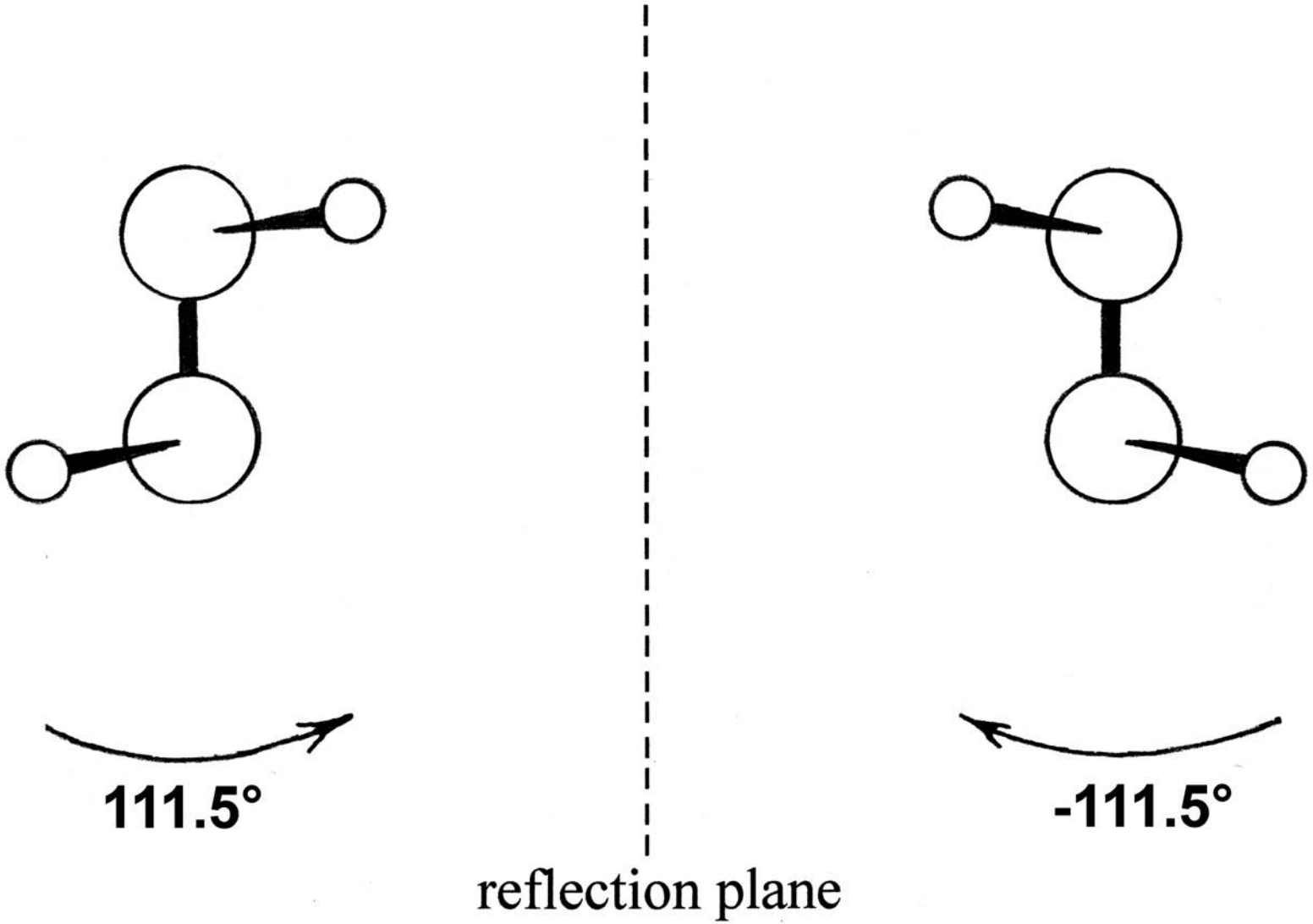

View 5

BACK

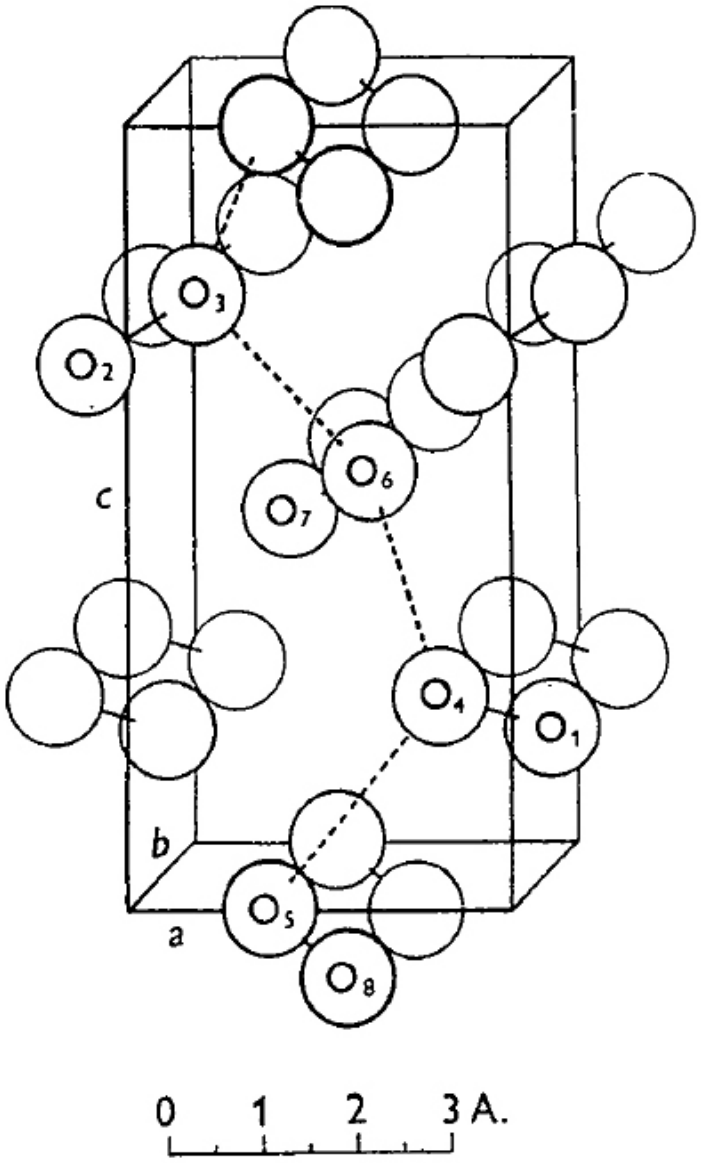


Fig. 6. An isometric view of the structure, with the *Internationale Tabellen*... origin.

View 6

BACK

# Flexible Tetramer Model, Stable Structures

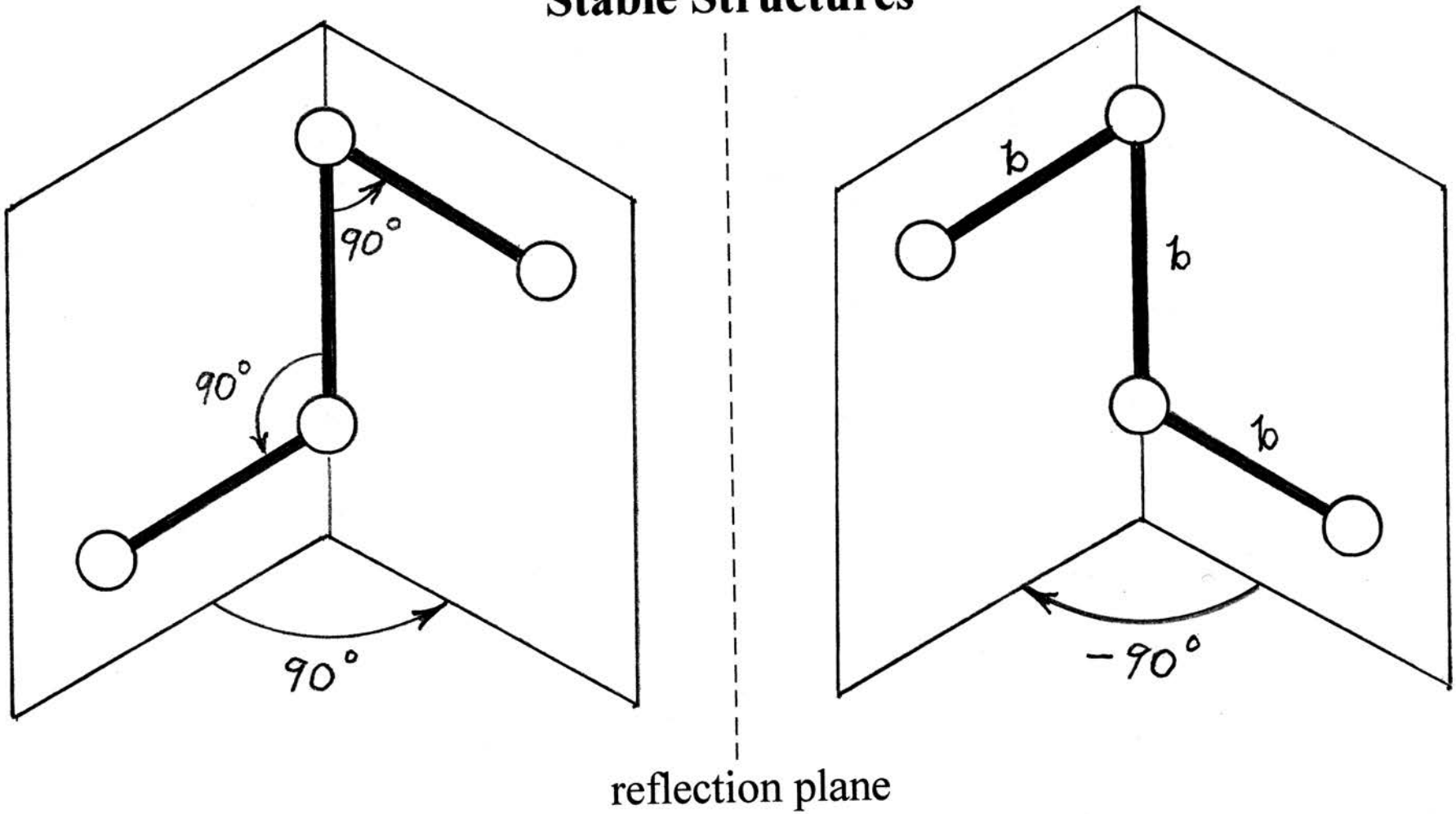

# Tetramer Intramolecular Potential Energy



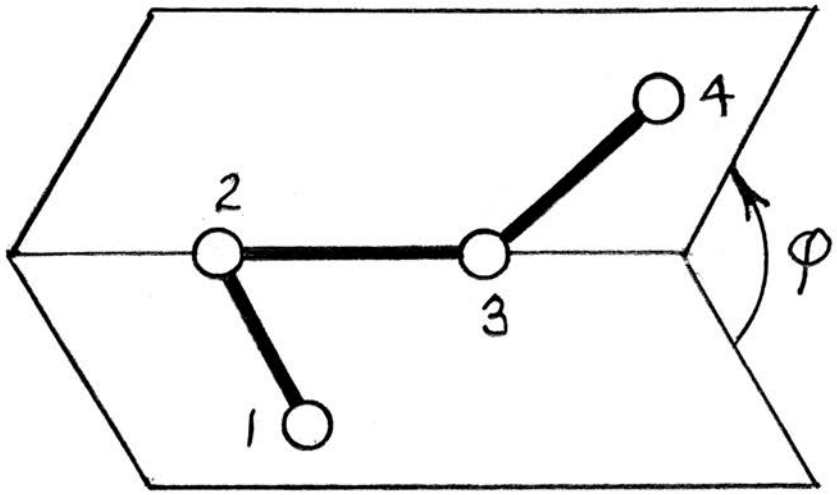


$$\Phi^{(1)}(\mathbf{r}_1,\mathbf{r}_2,\mathbf{r}_3,\mathbf{r}_4) = \sum_{i=1}^{3}(K_{str}/2)(r_{i,i+1}-b)^2 + \sum_{i=2}^{3}(K_{bnd}/2)(\theta_i-\pi/2)^2 + K_{dih}\cos^2\varphi \quad .$$

Dihedral angle $-\pi \le \varphi \le \pi$ definition:

$$\cos\varphi = \frac{(\mathbf{r}_{12}\times\mathbf{r}_{23})\cdot(\mathbf{r}_{23}\times\mathbf{r}_{34})}{|\mathbf{r}_{12}\times\mathbf{r}_{23}||\mathbf{r}_{23}\times\mathbf{r}_{34}|} \quad .$$

## Distinct Planar Transition States, Isolated Tetramer

- $\varphi = 0$ :

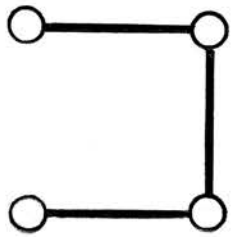

- $\varphi = \pm\pi$ :

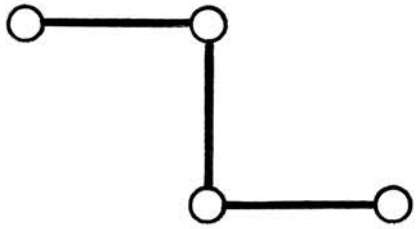

- Transition state barrier height: $K_{dih}$

- Harmonic normal mode frequencies at each transition state:
  five positive, six vanishing, one imaginary (reaction path)

# Chirality Measure for Individual Tetramers

- Monomers located at $\mathbf{r}_1, \mathbf{r}_2, \mathbf{r}_3, \mathbf{r}_4$ .
- $\zeta(\mathbf{r}_1,\mathbf{r}_2,\mathbf{r}_3,\mathbf{r}_4) = \dfrac{\mathbf{r}_{12}\cdot(\mathbf{r}_{23}\times\mathbf{r}_{34})}{|\mathbf{r}_{12}||\mathbf{r}_{23}||\mathbf{r}_{34}|} \equiv \dfrac{\mathbf{r}_{43}\cdot(\mathbf{r}_{32}\times\mathbf{r}_{21})}{|\mathbf{r}_{43}||\mathbf{r}_{32}||\mathbf{r}_{21}|}$ .
- $-1 \le \zeta \le +1$ ; $\zeta = \pm 1$ at the $\Phi^{(1)}$ minima .
- $\zeta = 0$ for tetramer planar configurations, including the ideal transition states.

# Tetramer Pair Interaction ($\Phi^{(2)}$)

- Sixteen energy-scaled Lennard-Jones pair interactions between monomers belonging to different tetramers ($\alpha$, $\gamma$):

$$\Phi^{(2)} = \sum_{i=1}^{4}\sum_{j=1}^{4} \varepsilon_{tt}(\zeta^{(\alpha)}, \zeta^{(\gamma)}) \mathrm{v}_{\mathrm{LJ}}(|\mathbf{r}_i^{(\alpha)} - \mathbf{r}_j^{(\gamma)}|/\sigma_{tt}) \quad .$$

- $\mathrm{v}_{\mathrm{LJ}}(x) = 4(x^{-12} - x^{-6})$ .

- $\varepsilon_{tt}(\zeta^{(\alpha)}, \zeta^{(\gamma)}) = \varepsilon_0(1 + \lambda\zeta^{(\alpha)}\zeta^{(\gamma)})$ , $\lambda > 0$ favors like enantiomers, $\lambda < 0$ favors opposite enantiomers.

- $\varepsilon_{tt}$ varies smoothly as the tetramers deform, passing through $\varepsilon_0$ when one tetramer changes chirality.

# Parameter Choice, Physical Units

- Backbone bond length: $b = 1.18\,\text{Å}$
- Backbone bond stretch force constant: $K_{str} = 1000$ kcal/mol Å$^2$
- Bond bend force constant: $K_{bnd} = 1000$ kcal/ mol rad$^2$
- Dihedral angle deformation constant: $K_{dih} = 2.775$ kcal/mol
- Monomer mass: $m = 8.5$ g/mol
- Lennard-Jones energy: $\varepsilon_0 = 0.15535$ kcal/mol
- Lennard-Jones length: $\sigma_{tt} = 1.115\,\text{Å}$

# Parameter Choice, Reduced Units

Elementary parameter set choice: $m$, $\varepsilon_0$, $\sigma_{tt}$

Time unit: $\sigma_{tt}(m/\varepsilon_0)^{1/2} = 0.4033\,\mathrm{ps}$

Number density unit: $\sigma_{tt}{}^{-3} = 0.7214\,\text{Å}^{-3} = 1198\,\mathrm{mol/l}$

Temperature unit: $\varepsilon_0 / k_B = 78.15\,\mathrm{K}$

Pressure unit: $\varepsilon_0 / \sigma_{tt}{}^{3} = 7786\,\mathrm{bar}$

Dimensionless intramolecular ($\Phi^{(1)}$) parameters:

$$K_{str} = 8002, \quad K_{bnd} = 6437, \quad K_{dih} = 17.86, \quad b = 1.0583$$

View 13

BACK

# Ground State for Two Tetramers with an Enantiopure Bias

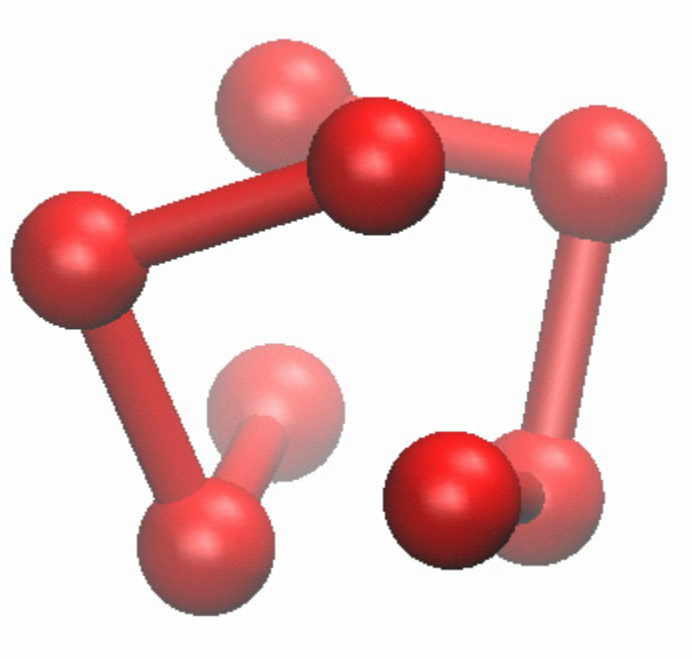

$\Phi = -13.18$

View 14

BACK

# Ground State for Two Tetramers with a Racemic Bias

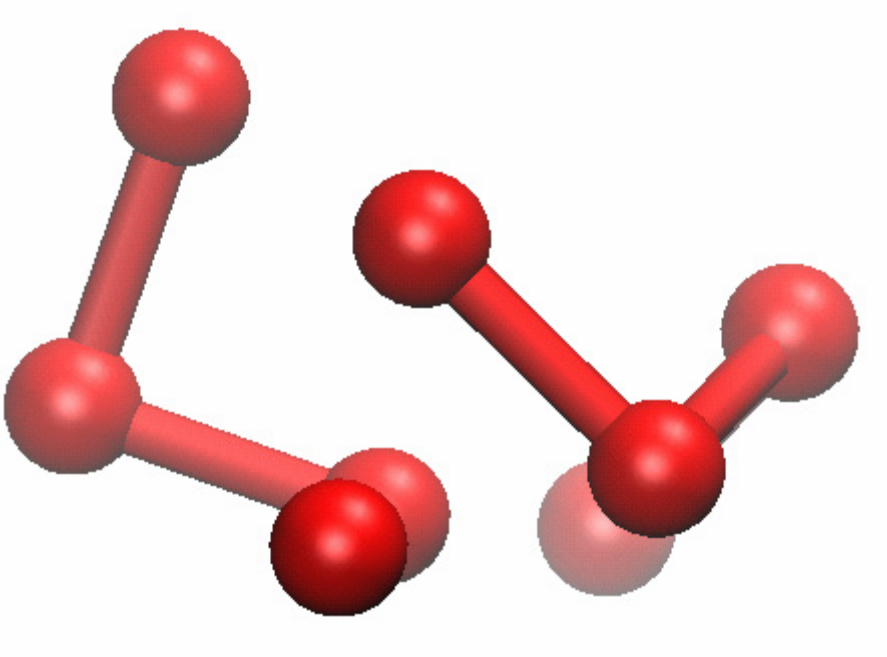

$$\Phi = -12.86$$

# Simple Achiral Solvent for Tetramers

- Lennard-Jones 12,6 pair potentials are postulated for monomer-solvent and for solvent-solvent interactions:

  monomer-solvent: $\varepsilon_{ts} v_{LJ}(r/\sigma_{ts})$ ($\zeta$-independent) ,

  solvent-solvent: $\varepsilon_{ss} v_{LJ}(r/\sigma_{ss})$ .

- Additional simplifications: $\varepsilon_{ts} = \varepsilon_{ss} = \varepsilon_0$ , and $\sigma_{ss} = \sigma_{ts} = \sigma_{tt}$ , so that all L-J pair potentials involving solvent are identical.

# Inter-conversion of a single tetramer in a Lennard Jones fluid

**(reduced number density = 0.6624)**

View 16

BACK

T = 4.0

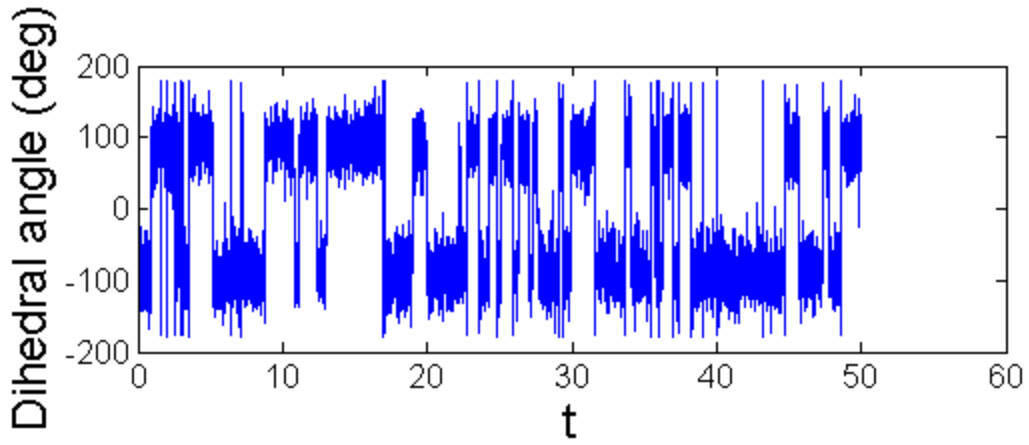


T = 2.0

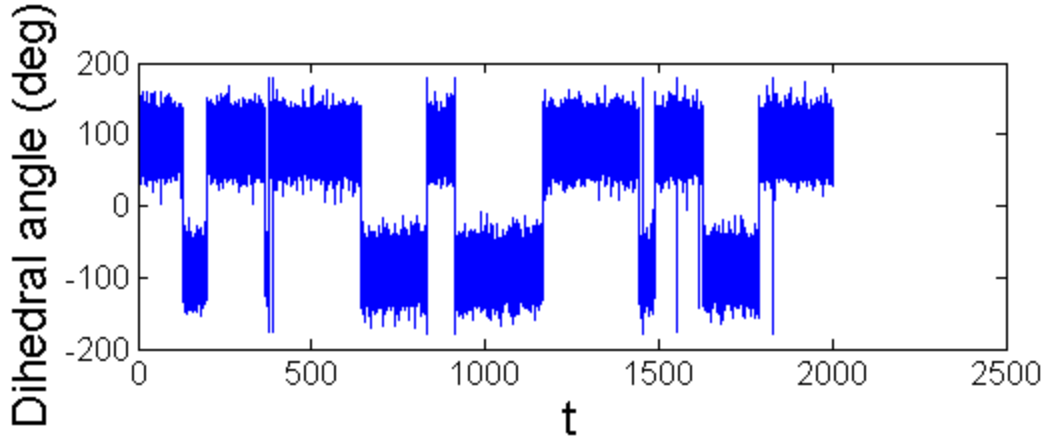

# Autocorrelation Function of Chirality Measure

$$C(t)=\langle \zeta(t_0+t)\zeta(t_0)\rangle / \langle \zeta^2(t_0)\rangle$$



T = 4.0

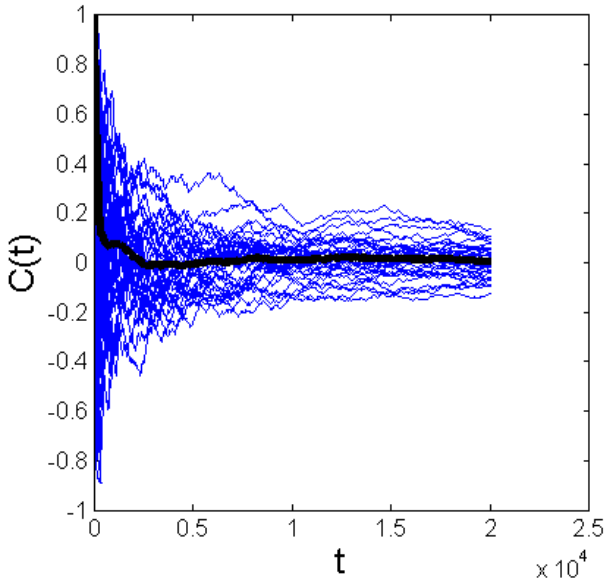


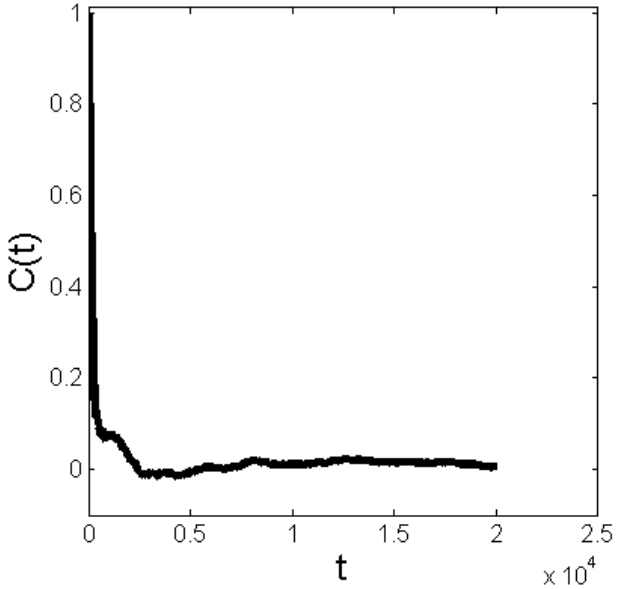


T = 2.0

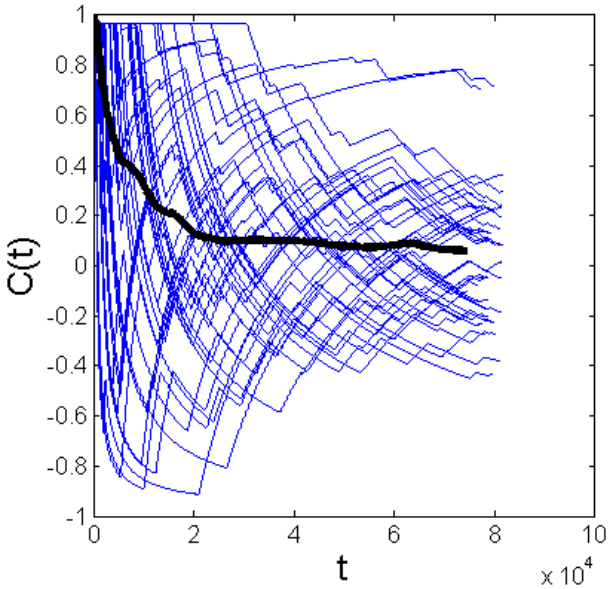


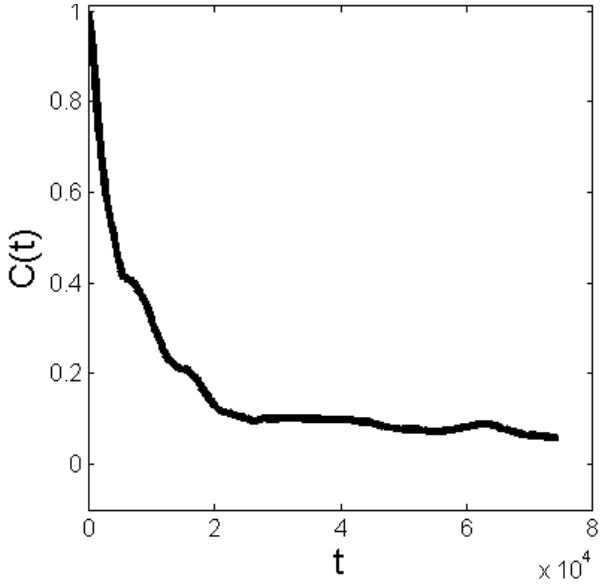

# Resolved Transition Rates for the Transition States (reduced number density = 0.6624)

View 18

BACK

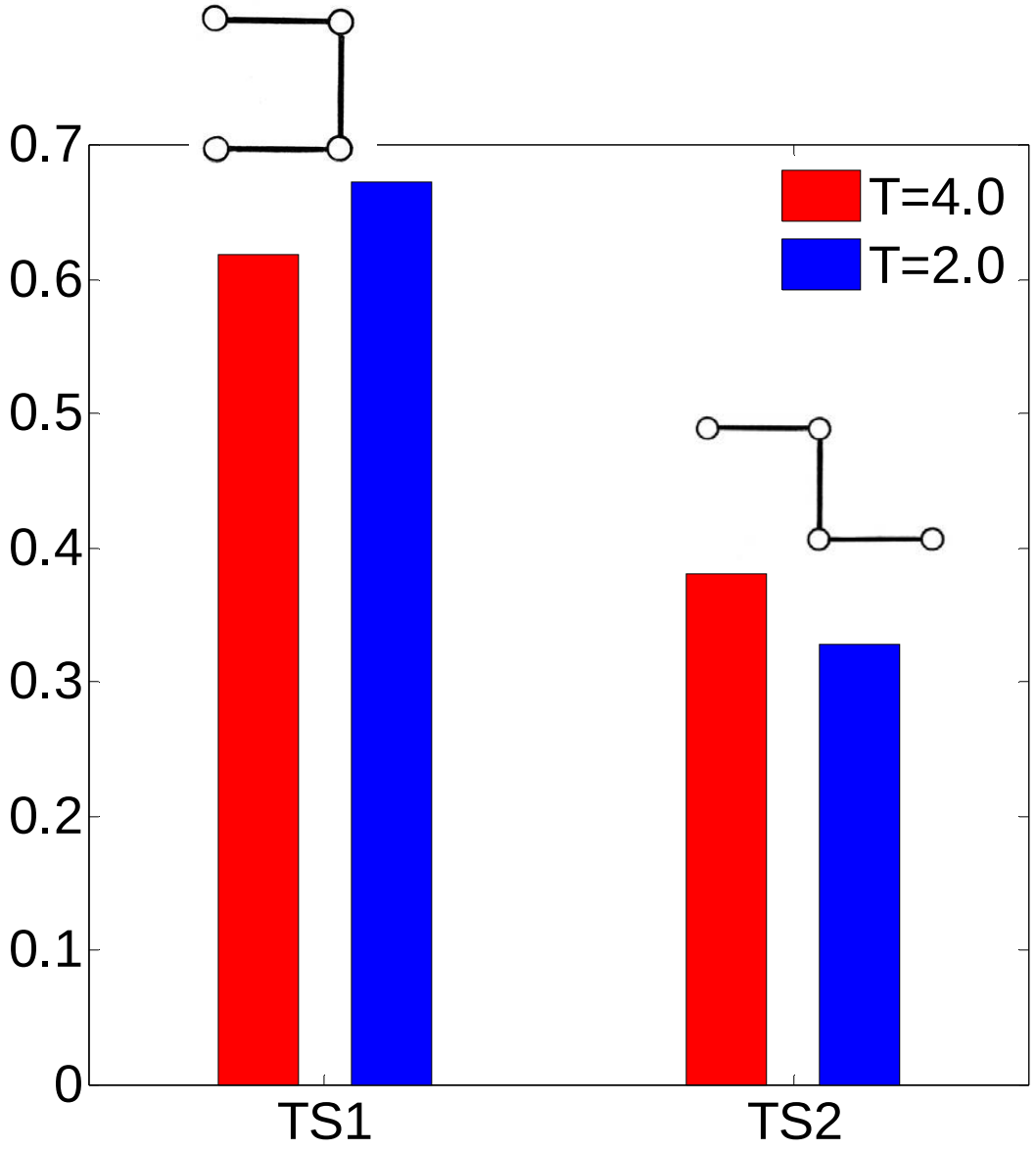

# Immiscible Pairs of Isotropic Chiral Liquids

Reference:

C. Dressel, T. Reppe, M. Prehm, M. Brautzsch, and C. Tschierske, *Nature Chemistry* **6**, 971-977 (2014), "Chiral self-sorting and amplification in isotropic liquids of achiral molecules".

Molecular structure (R = *n* - $C_6H_{13}$):

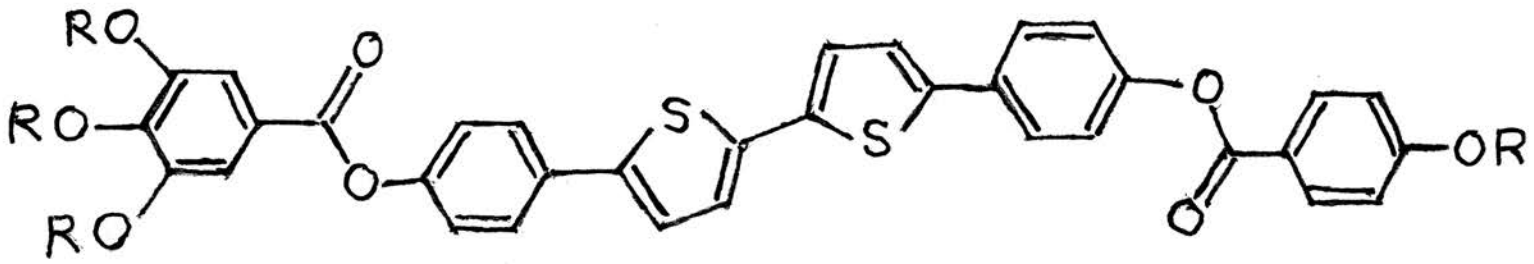


Approximate temperature range of immiscibility: $180^\circ C \leq T \leq 205^\circ C$

View 20

BACK

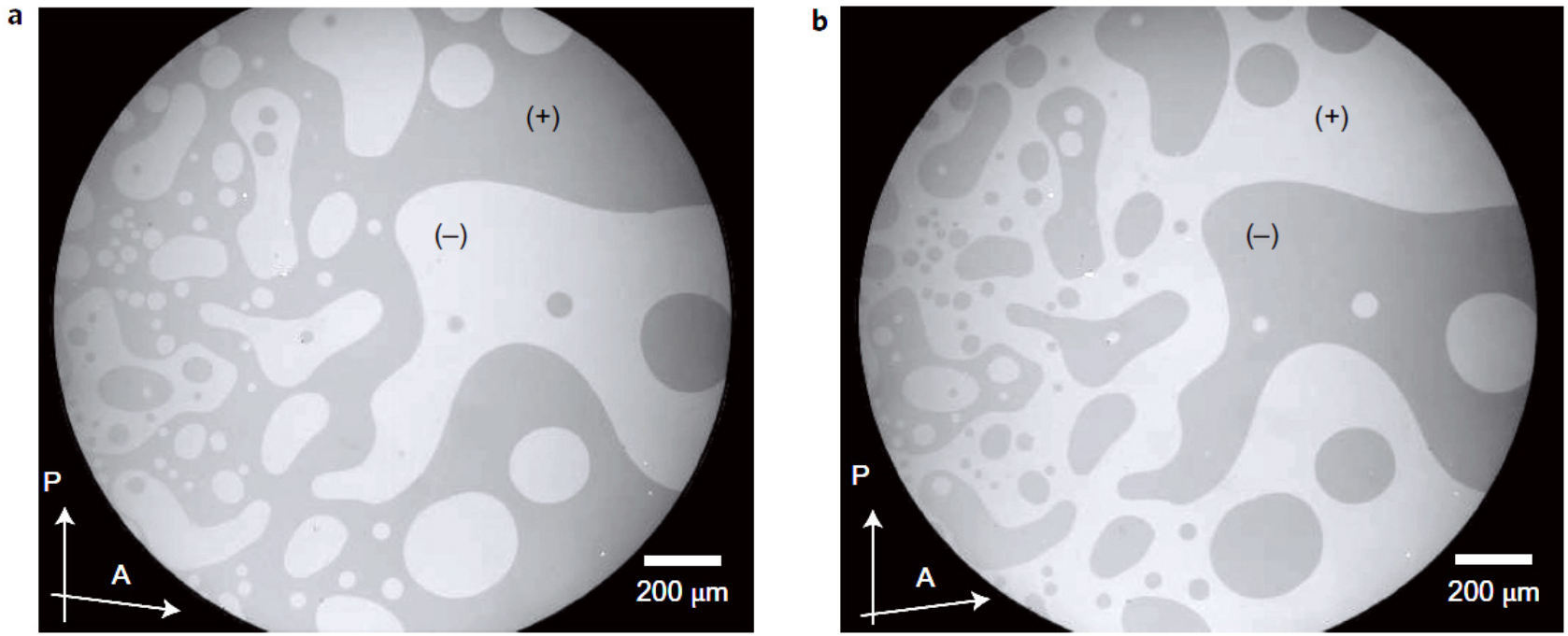

# Time dependence of average chirality at high temperature, T= 4.0

**(reduced tetramer number density = 0.17)**

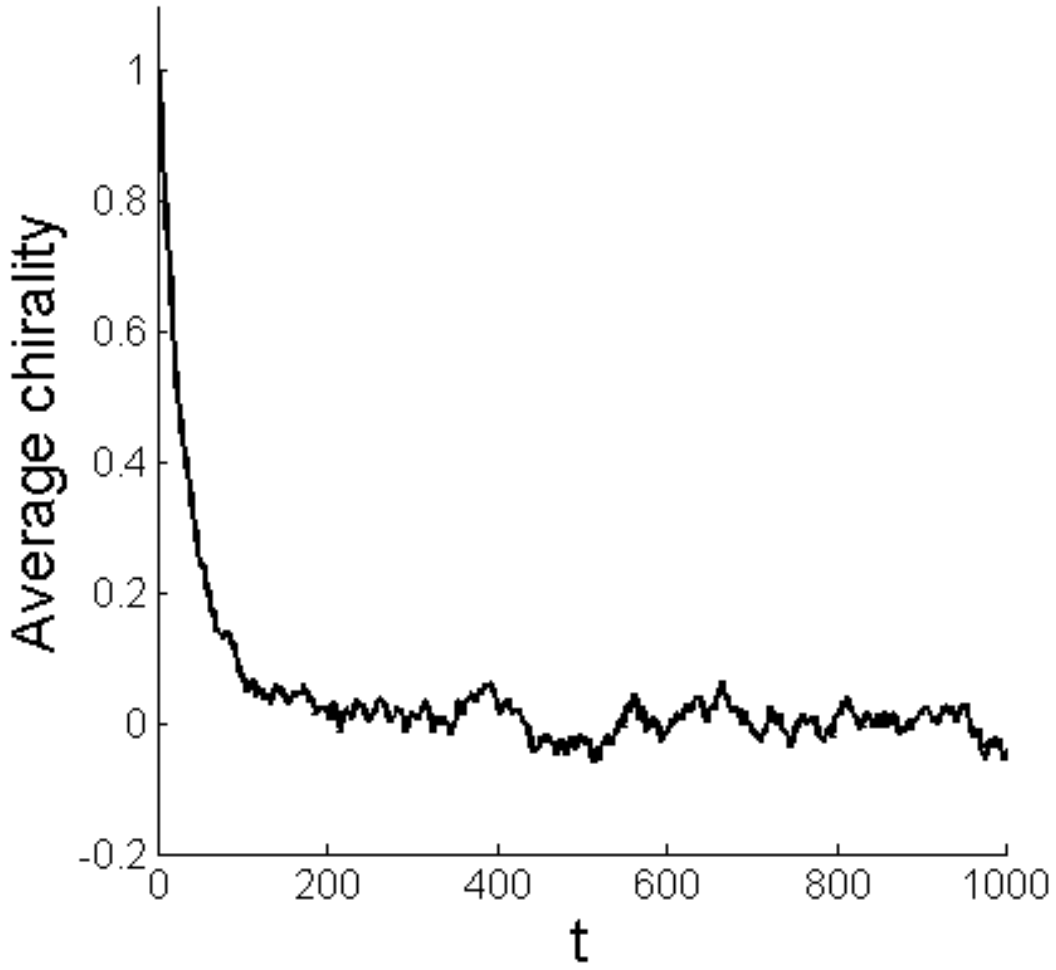

# Average chirality at low temperature, T= 1.4

**(reduced tetramer number density = 0.17)**

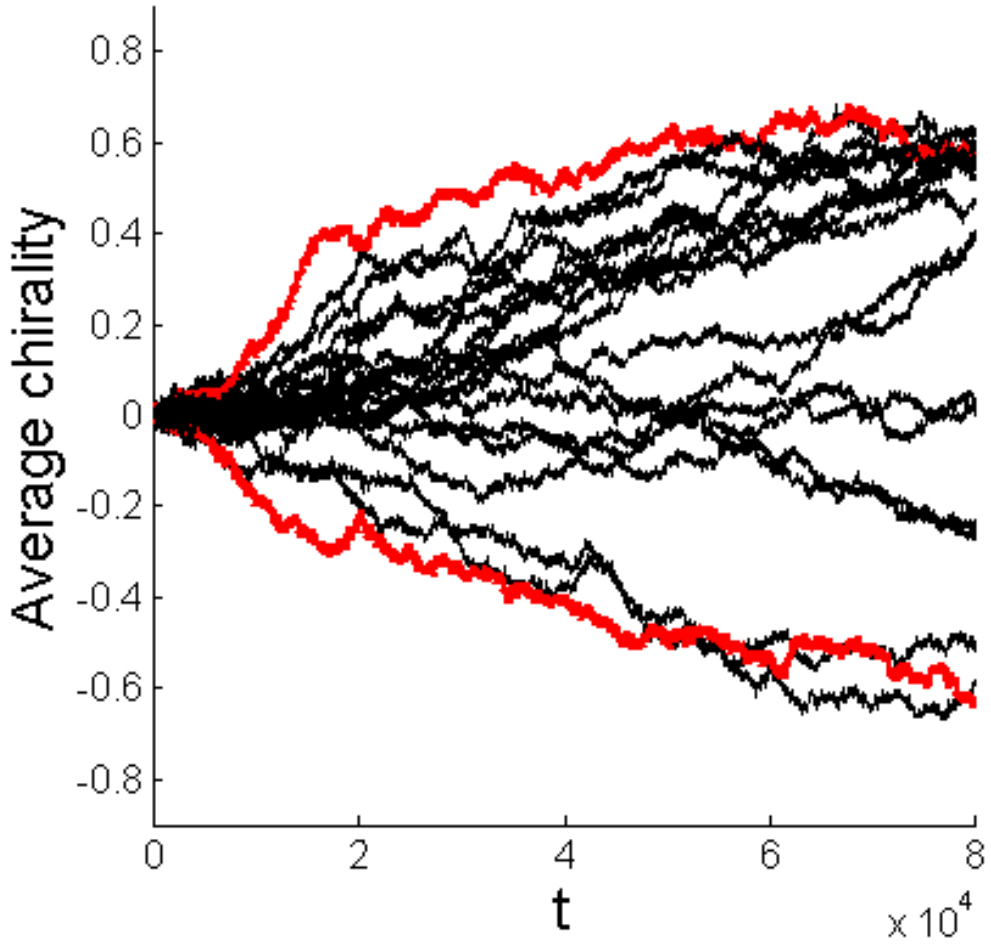

BACK

# Time dependence of average chirality at low temperature, T= 1.4

**(reduced tetramer number density = 0.17)**

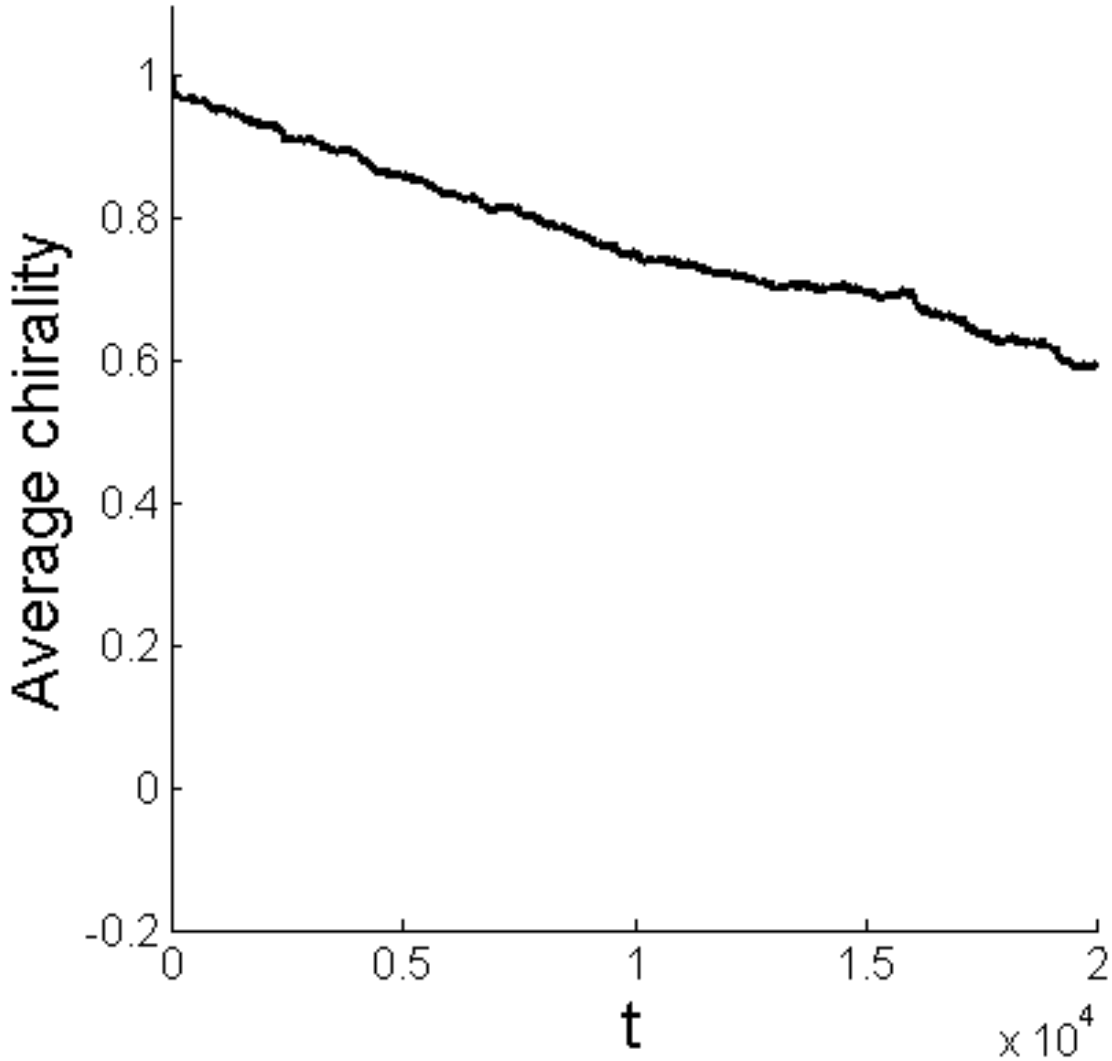

View 24

BACK

# Prototype Crystal Structure: Enantiopure Simple Cubic

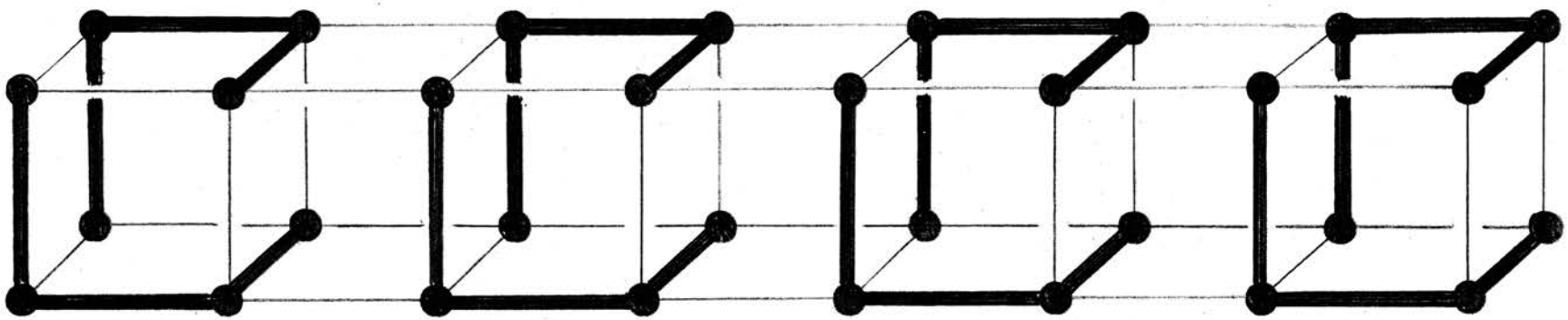

$\rho_{tetr} = 0.210920$ ,  $\Phi / N_{tetr} = -20.6595$

View 25

BACK

# Inherent structure for simple cubic crystal, T= 0.01

**(128 tetramers)**

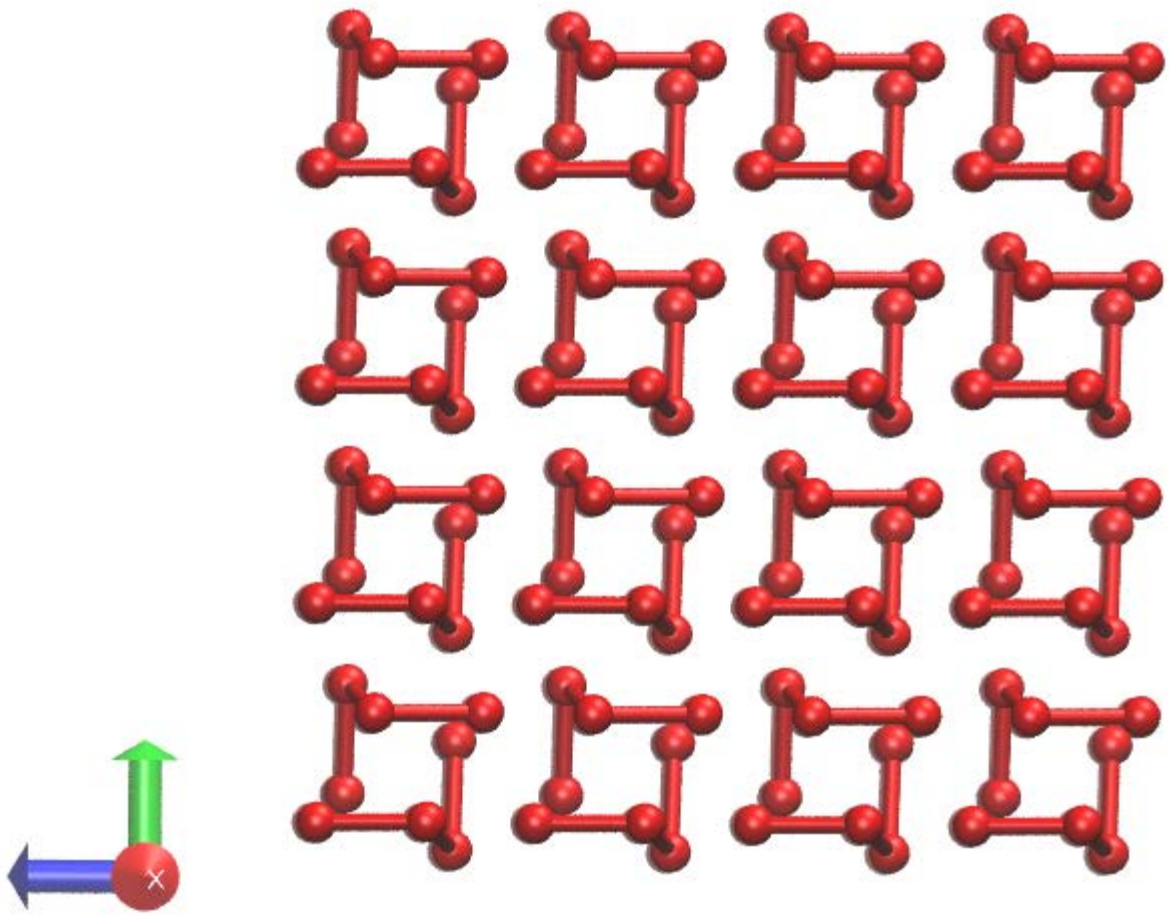

$$\Phi / N_{tetr} = -29.1$$

$$\rho_{tetr} = 0.24$$

# Inherent structure for simple cubic crystal, T= 0.01

**(128 tetramers)**

View 26

BACK

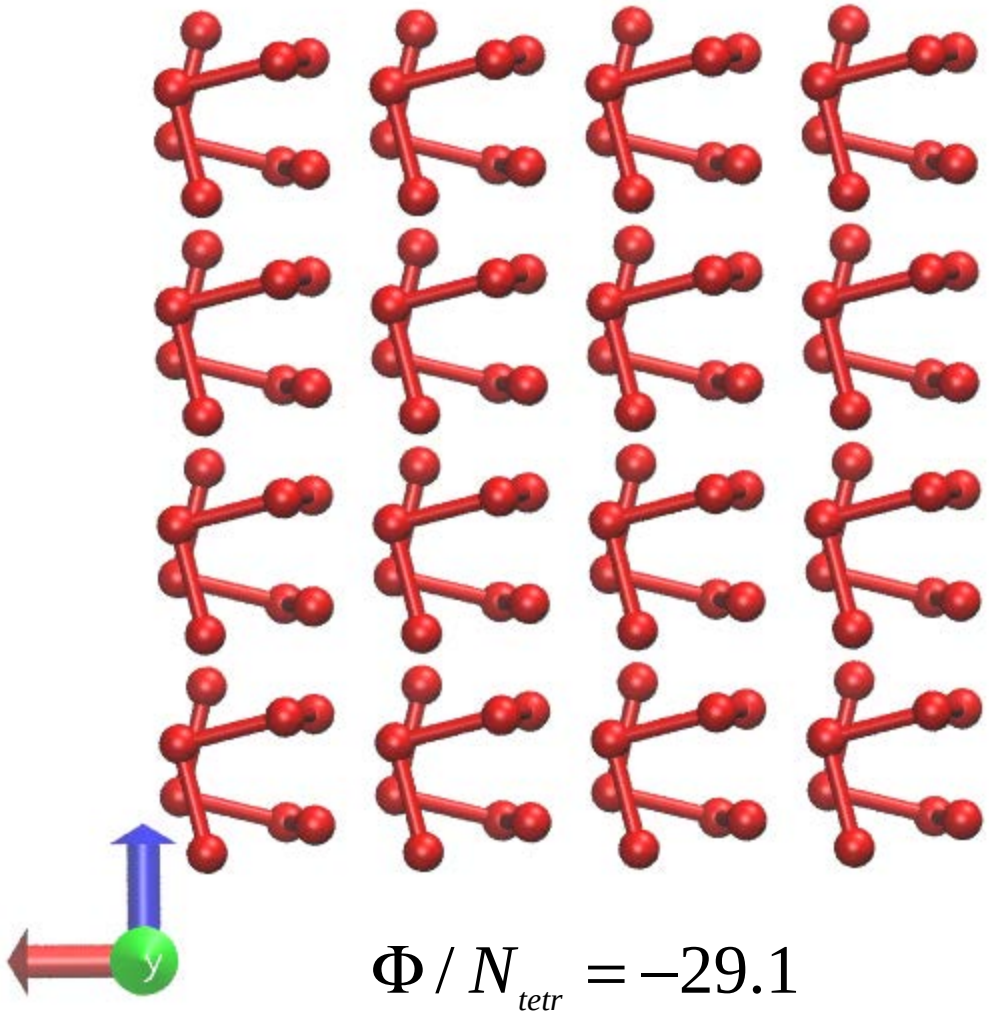


$$\Phi / N_{tetr} = -29.1$$

$$\rho_{tetr} = 0.24$$

# Inherent structure for simple cubic crystal, T= 0.01

**(128 tetramers)**

View 27

BACK

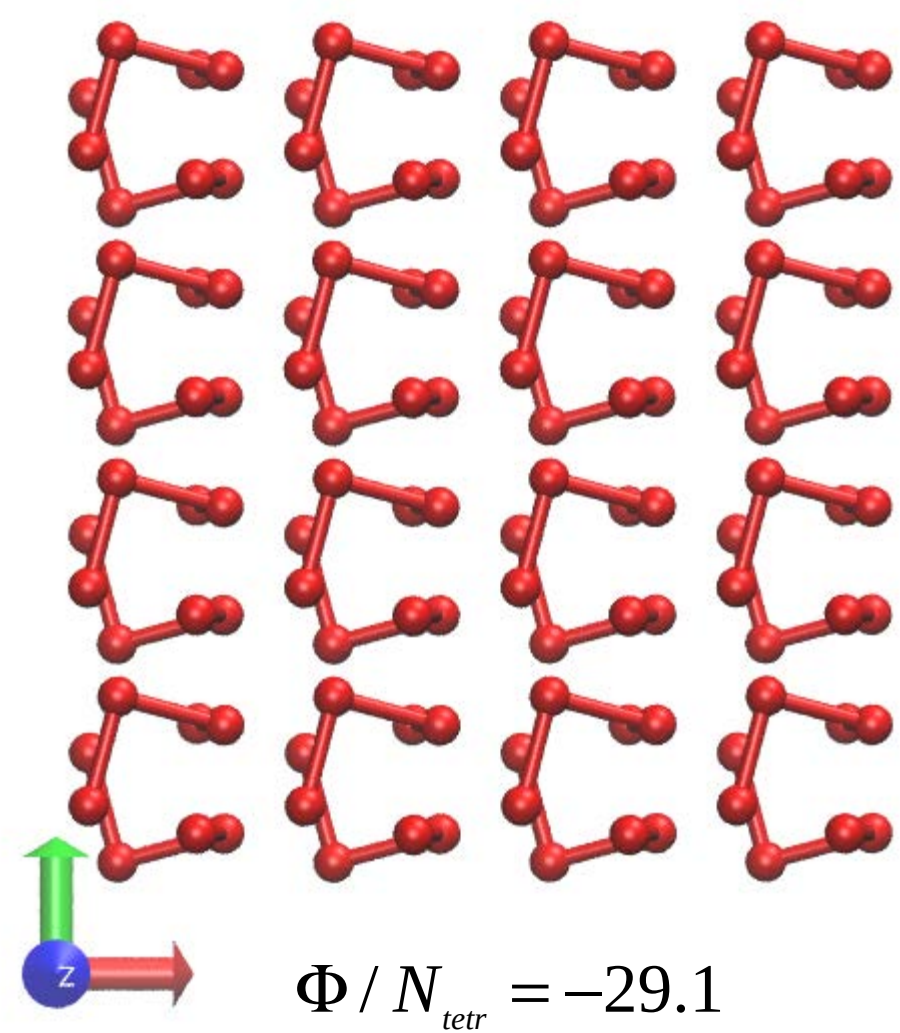


$$\Phi / N_{tetr} = -29.1$$

$$\rho_{tetr} = 0.24$$

View 28

BACK

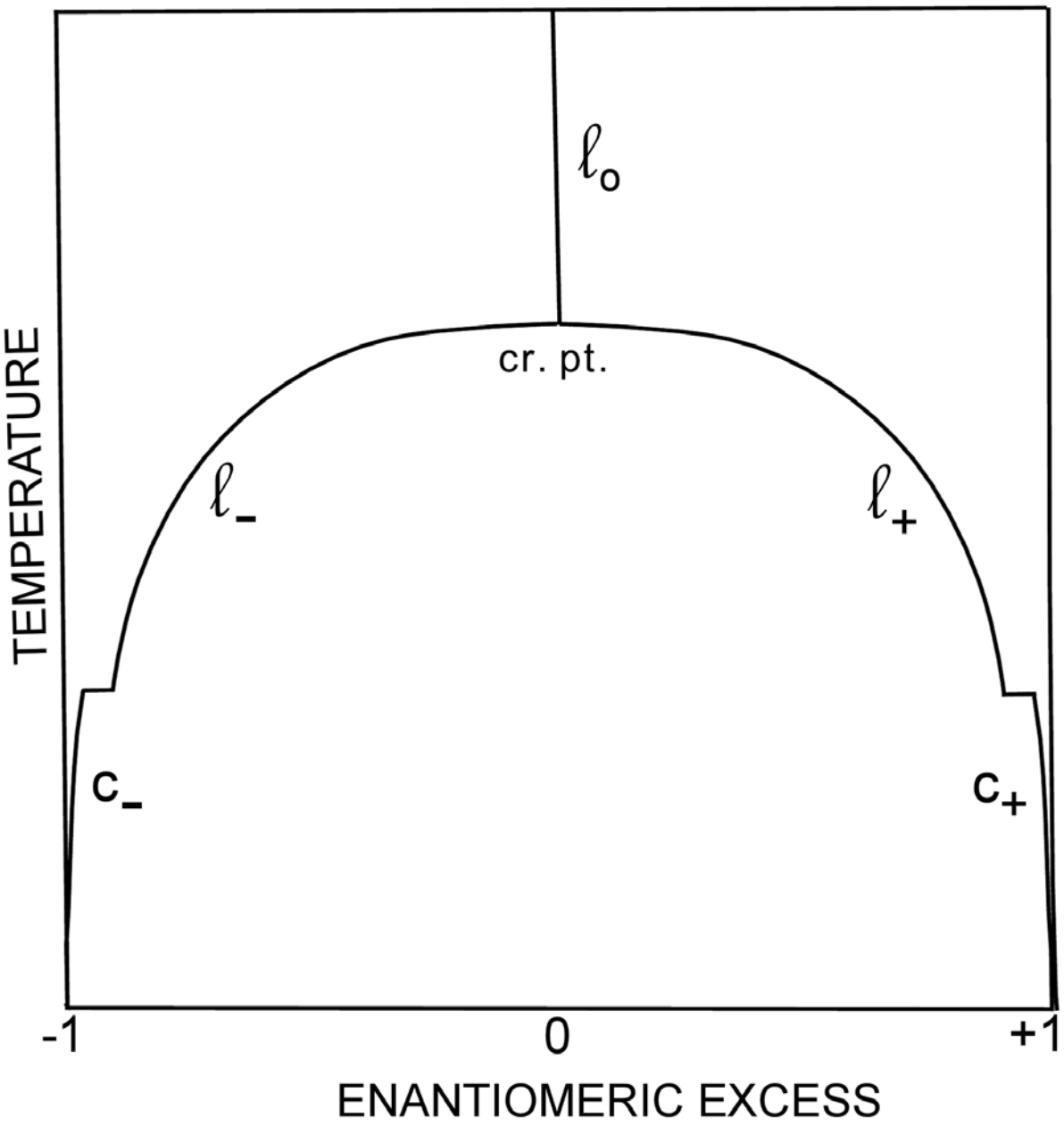

# Chirality-renormalized pair potential

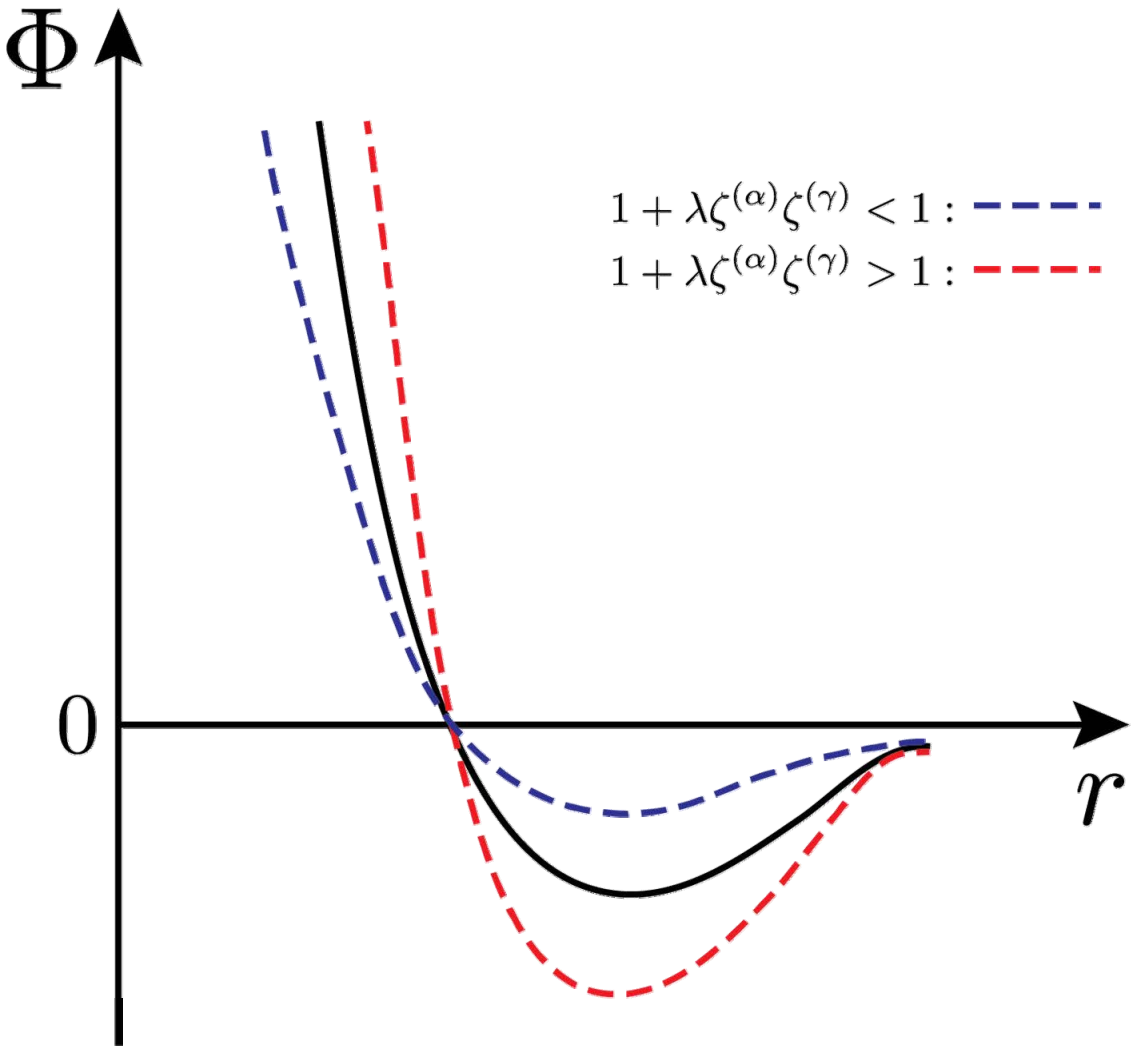

# Phase separation of chiral liquids at a low temperature, T= 1.4

BACK

**(reduced tetramer number density = 0.17)**

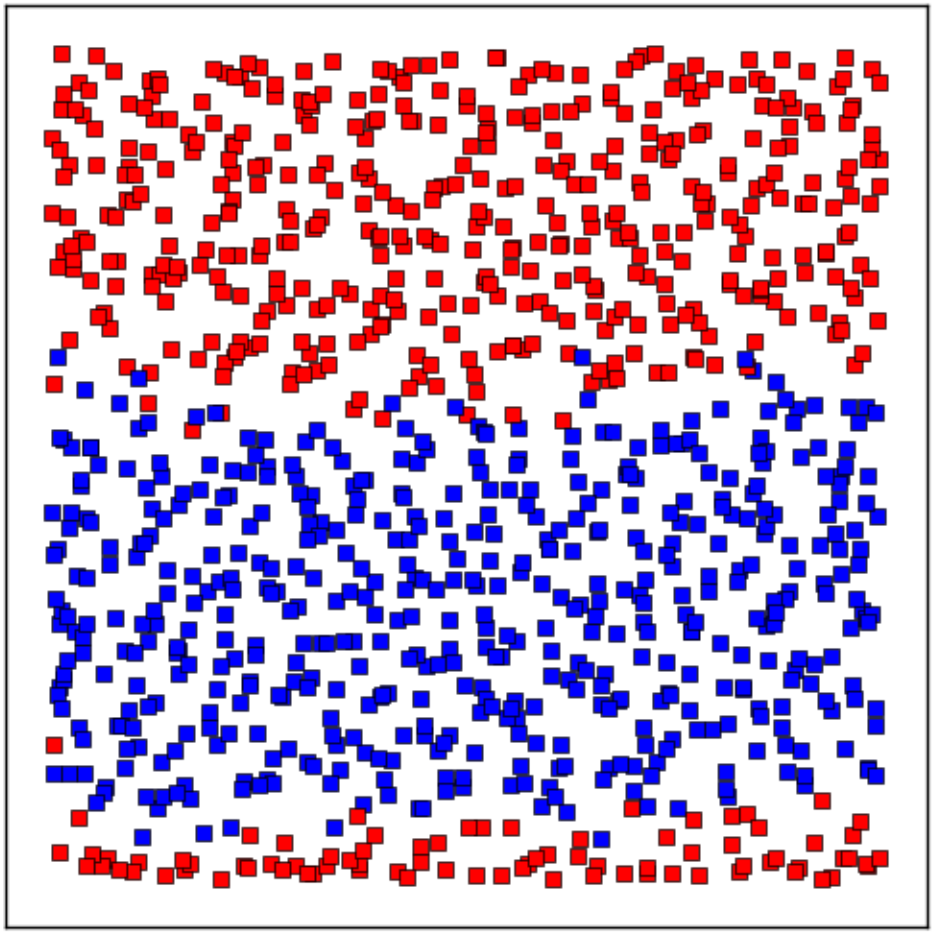

# Ostwald Ripening Phenomenon

Original reference: W. Ostwald, Lehrbuch der Allgemeinen Chemie, vol. 2, part 1 (Leipzig, Germany, 1896).

Physical phenomenon: In a collection of crystals of various sizes, a driving force exists for the large crystals to add material at the expense of the small crystals.

Gibbs-Thompson effect: Interfacial free energy increases the chemical potential of a cluster (crystal, droplet, ....) above that of the bulk phase. For a compact cluster with radius R that increase is proportional to $R^{-1/3}$. This creates a liquid droplet analog of Ostwald crystal ripening.

# Viedma Ripening Phenomenon

[crystal slurry deracemization driven by vigorous stirring with glass beads]

1. Viedma, C., *Phys. Rev. Lett.* **94**, 065504 (2005), "Chiral Symmetry Breaking During Crystallization: Complete Chiral Purity Induced by Nonlinear Autocatalysis and Recycling".

2. Viedma, C., Ortiz, J.E., Torres, T., Izumi, T., and Blackmond, D., *J. Am. Chem. Soc.* **130**, 15274-15275 (2008), "Evolution of Solid Phase Homochirality for a Proteinogenic Amino Acid".

3. Hein, J.E., Cao, B.H., Viedma, C., Kellog, R.M., and Blackmond, D.G., *J. Am. Chem. Soc.*, **134**, 12629-12636 (2012), " Pasteur's Tweezers Revisited: On the Mechanism of Attrition-Enhanced Deracemization and Resolution of Chiral Conglomerate Solids".

# Tetramer Model: Future Applications

- Self-diffusion constant $D$ and shear viscosity $\eta$ for both the racemic and the chiral-symmetry-broken liquids.

- How well is the Stokes-Einstein relation obeyed?

$$D\eta = \frac{k_B T}{Ca_{hydro}}$$

- $T$ dependence of surface tension for coexisting chiral liquids, and for coexisting liquid-vapor interfaces.

- Rotation of polarized light by chiral liquids, assuming anisotropic polarizability for each tetramer covalent bond.

- Low-T crystal structure phase transitions as $p$ increases, for both the $\lambda > 0$ and the $\lambda < 0$ cases.

# Future Modeling Research Opportunities

- Accurate quantum mechanical calculations of real enantiomer intramolecular and intermolecular interactions.
- Develop simple MD model for C* stereochemistry kinetics.
- Biasing effect of a chiral solvent on symmetry breaking.
- Chemical bond formation between non-chiral reactants to form chiral molecular products, *e.g.*, 2 dimers ↔ tetramer .
- Catalytic effect of tetramer enantiomers on surrounding chemical synthesis reactions.
- Slowing effect of high solvent viscosity on chiral symmetry breaking, *e.g.*, approach to a solvent glass transition.